

# UniRestorer: Universal Image Restoration via Adaptively Estimating Image Degradation at Proper Granularity

Jingbo Lin<sup>1</sup>, Zhilu Zhang<sup>1</sup>, Wenbo Li<sup>2</sup>, Renjing Pei<sup>2</sup>, Hang Xu<sup>2</sup>, Hongzhi Zhang<sup>1</sup>, Wangmeng Zuo<sup>1</sup>  
<sup>1</sup>Harbin Institute of Technology <sup>2</sup>Huawei Noah’s Ark Lab

## Abstract

Recently, considerable progress has been made in all-in-one image restoration. Generally, existing methods can be degradation-agnostic or degradation-aware. However, the former are limited in leveraging degradation-specific restoration, and the latter suffer from the inevitable error in degradation estimation. Consequently, the performance of existing methods has a large gap compared to specific single-task models. In this work, we make a step forward in this topic, and present our UniRestorer with improved restoration performance. Specifically, we perform hierarchical clustering on degradation space, and train a multi-granularity mixture-of-experts (MoE) restoration model. Then, UniRestorer adopts both degradation and granularity estimation to adaptively select an appropriate expert for image restoration. In contrast to existing degradation-agnostic and -aware methods, UniRestorer can leverage degradation estimation to benefit degradation-specific restoration, and use granularity estimation to make the model robust to degradation estimation error. Experimental results show that our UniRestorer outperforms state-of-the-art all-in-one methods by a large margin, and is promising in closing the performance gap to specific single-task models. The code and pre-trained models will be publicly available at <https://github.com/mrluin/UniRestorer>.

## 1. Introduction

Image restoration is a fundamental task in computer vision, it aims to restore high-quality (HQ) images from corresponding low-quality (LQ) counterparts, including denoising [1, 106], deblurring [61, 70, 107], de-weathering [23, 51, 55, 96], low-light enhancement [83, 89, 108], etc. In the past decade, advanced deep neural architectures [27, 56, 67, 80, 105] have driven image restoration methods to evolve from task-specific [20, 33, 54, 69, 76, 98] to task-agnostic [15, 46, 49, 94, 95] backbones. Recently, influenced by the success of foundation models in natural language processing and high-level vision, there has been in-

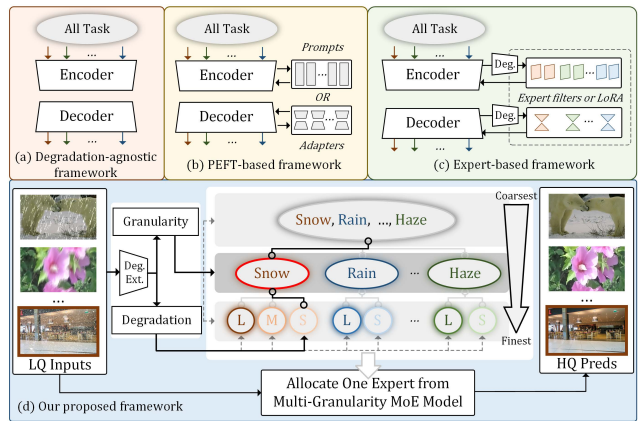


Figure 1. **Illustration of representative all-in-one image restoration frameworks.** (a) Degradation-agnostic methods [82, 100] train a shared backbone using data from all tasks and are limited in leveraging degradation-specific restoration. (b) PEFT-based methods [4, 25, 39, 64, 79, 87, 97] apply learnable prompts or adapters to the backbone to adapt various tasks. (c) Expert-based methods [11, 12, 14, 19, 45, 47, 63, 84, 90, 91, 112] train specific MoE, LoRA, or filters for specific tasks. However, both (b) and (c) suffer from the inevitable error in degradation estimation. (d) We construct a multi-granularity degradation space and a multi-granularity MoE restoration model. By adaptively estimating image degradation at proper granularity, our UniRestorer can be effective in leveraging degradation-specific restoration while being robust to degradation estimation error.

creasing interest in addressing multiple image restoration tasks within a single framework, known as all-in-one image restoration [31].

A straightforward approach is to utilize data from all tasks to train a degradation-agnostic model (see Fig. 1 (a)), but it easily yields unsatisfactory results due to the conflicts between certain tasks (e.g., denoising and deblurring). Inspired by parameter-efficient fine-tuning (PEFT) methods [9, 28], learnable prompts [25, 39, 64, 79, 87, 97] and adapters [4] are integrated into the restoration model to modulate intermediate features (see Fig. 1 (b)), enabling the model to process different tasks more specifically. Furthermore, some methods introduce mixture-of-experts (MoE) [12, 14, 45, 84, 91] (MoE-like using filters [11, 19, 47, 63, 90, 112] and low-rank adaptation [3,

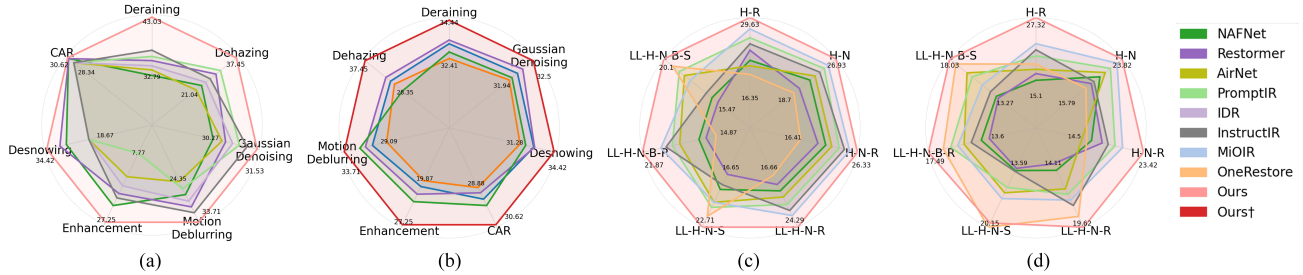


Figure 2. **Comparisons with task-agnostic methods, all-in-one methods, and task-specific models on all-in-one image restoration.** Ours and Ours† denote *auto* and *instruction* modes, which are respectively used for a fair comparison with all-in-one and specific single-task models. (a) Comparisons on single-degradation setting. (b) Comparisons with specific single-task models. (c) Comparisons on mixed-degradation setting (*in-distribution*). (d) Comparisons on mixed-degradation setting (*out-distribution*).

78]) modules, routing the current feature to specific experts based on deep features and the estimated degradation representations (DRs), as shown in Fig. 1 (c).

Despite rapid progress, these methods show limited performance, falling significantly behind specific single-task models. The degradation-agnostic models cannot leverage the benefits from degradation estimation based priors to improve all-in-one restoration performance. PEFT-based and MoE-based methods provide degradation-aware ways for processing different corruptions specifically conditioning on degradation estimation. However, their performance heavily relies on accurate degradation estimation, which is difficult due to the broad range of degradation space of all-in-one image restoration. Thus, it is inevitable for degradation-aware models suffering from errors in degradation estimation. Inaccurate estimation can cause images to be inappropriately processed by the model, resulting in decreased restoration performance.

From the above analysis, one plausible solution to improve all-in-one restoration is to estimate and leverage image degradation while being robust to degradation estimation error. As illustrated in Fig. 1 (d), we construct a multi-granularity degradation space and train one multi-granularity MoE restoration model. Besides vanilla degradation estimation, we introduce granularity estimation to indicate the degree of degradation estimation error. Intuitively, giving a snowy image, when the degradation is estimated with large error, granularity estimation will allocate a coarser-grained expert, *e.g.*, a desnowing model, for alleviating the effect of estimation error. When the degradation is precisely estimated, granularity estimation will allocate a finer-grained expert, *e.g.*, a model for light snow. Thus, using both degradation and granularity estimation, our method can adaptively allocate the appropriate expert to given unknown corrupted inputs. As a result, our method can effectively utilize the image degradation estimation while alleviating the negative affect caused by the error-prone degradation estimation.

Specifically, we take the following steps to implement our UniRestorer. First, we optimize a degradation extractor

that is aware of finer-grained image degradation. Second, all low-quality images in the training set are fed into the degradation extractor, and their features are then hierarchically clustered into multiple DR groups at different granularities respectively, which forms the multi-granularity degradation set shown in Fig. 3. Third, we train a multi-granularity MoE restoration model based on the constructed multi-granularity degradation set. Fourth, given an image with unknown degradation, we learn routers based on both degradation and granularity estimation results. The router identifies which DR group the degradation and granularity best match in the degradation set, and then allocates the corresponding expert for inference.

To demonstrate the effectiveness and universality of the proposed method, we conduct experiments on both single-degradation and mixed-degradation images. For the single-degradation setting, we unify 7 common image restoration tasks. For the mixed-degradation setting, we introduce 6 degradation types. Furthermore, we conduct a comprehensive comparative evaluation. The results indicate that our method not only significantly outperforms existing all-in-one methods but also achieves performance that is competitive with, or even superior to, specific single-task models.

The main contributions can be summarized as follows:

- We propose to learn all-in-one image restoration in multiple granularities. Specifically, we train a multi-granularity MoE restoration model, which simultaneously maintains superior restoration performance and good generalization ability.
- To alleviate the effect of degradation estimation error, we propose to estimate image degradation at proper granularity. Based on both degradation and granularity estimation, we can allocate the most appropriate expert for unknown corruptions.
- Extensive experiments conducted on both single-degradation and mixed-degradation images show that our method significantly outperforms existing all-in-one methods and effectively closes the performance gap with specific single-task models.

## 2. Related Work

**Image Restoration for Specific Tasks.** Pioneer works propose tailored frameworks for specific degradations, *e.g.*, DnCNN [98] for denoising, SRCNN [20] for super-resolution, DeblurGANv2 [33] for deblurring, PReNet [69] for draining, Dehazeformer [76] for dehazing, and DesnowNet [?] for desnowing. Benefits from advanced deep neural networks, some works tend to develop task-agnostic models, such as MPRNet [94], SwinIR [46], NAFNet [15], and Restormer [95], which become strong baselines in various image restoration tasks. Although significant progress achieved, these models still need to train or fine-tune independent models for specific degradations, resulting in additional computational costs.

**PEFT-based All-in-One Image Restoration.** To adapt to various corruptions, pioneer all-in-one image restoration methods [4, 39, 64, 79, 87, 97] integrate PEFT-based techniques into the restoration backbone. For example, TransWeather [79] introduces learnable weather-type oriented embeddings as prompts to modulate decoder feature, unifying multiple bad weather restoration tasks. AirNet [39] generates degradation-specific prompts via contrastive learning and adjusts features based on different corruptions. Similarly, PromptIR [64] employs prompt learning in a more powerful backbone [95] and achieves state-of-the-art performance. IDR [97] transforms a set of task-oriented knowledge hubs into a prompt via learnable PCA, effectively guiding the restoration model. Based on pre-trained StableDiffusion (SD), M-Perciever [4] develops a dual-branch multimodal prompts (*i.e.*, text prompt and visual prompt) as SD priors to guide SD model in all-in-one image restoration task. MiOIR [87] utilizes explicit prompt and adaptive prompt learning together to adapt to different tasks flexibly. Albeit successfully unifying various tasks, previous methods have limited performance and perform much worse than single-task models.

**Expert-based All-in-One Image Restoration.** As a basic component in modern deep learning architecture, Mixture-of-Experts (MoE) [30, 32] has been proven to be an efficient technique for training gigantic models [22, 36, 60, 71, 72, 74] and a solution to multi-task learning (MTL) due to its conditional processing capability [16, 17, 111]. Although prompt learning-based techniques can work similarly to MoE in conditional processing, they are still limited in performance and task range. Instead of conditional feature modulation, MoE directly allocates specific weights to each task. Recent MoE-based all-in-one image restoration methods fall into implicit MoE [11, 19, 47, 63, 90, 93, 112] and explicit MoE [14, 45, 78, 84, 91]. Which related to ours are the methods explicitly employing MoE-like modules in their framework and learning pipeline. For example, GRIDS [12] divide one complete degradation space into several intra-related subspaces and learn specific ex-

perts for each to alleviate potential conflicts among different degradations. Instruct-IPT [78] introduces individual adapters [29] for each task, by combining knowledge of the shared backbone and knowledge of task-specific adapters, which enables the all-in-one model to adapt to different tasks effectively. RestoreAgent [14] develops an expert pool that contains multiple single-task experts, and then it integrates the expert pool with multimodal large language models (MLLM) to form a human-interactable image restoration system. Albeit achieving rapid progress, it is difficult to estimate an accurate and fine-grained DR for given corrupted inputs, and the inaccurate routing could impede the restoration performance.

## 3. Proposed Method

In this section, we introduce our all-in-one image restoration framework, UniRestorer. We first optimize one degradation representation (DR) extractor that learns DRs at a finer-grained level, *i.e.*, degradation ‘DEGREE’. Based on DRs extracted from all low-quality training data, we conduct hierarchical data clustering that separates DRs into multiple DR groups at different granularities, *i.e.*, ‘ALL’, ‘TYPE’, and ‘DEGREE’ (see Fig. 3), leading to a multi-granularity degradation set and MoE restoration model. To alleviate the inevitable error caused by degradation estimation in routing, we adopt both degradation and granularity estimation to allocate the most appropriate expert to given unknown corrupted inputs.

We first give a preliminary knowledge of the Mixture-of-Experts in Sec. 3.1. In Sec. 3.2, we introduce the training of fine-grained DR extractor for given corrupted inputs  $\mathbf{X} \in \mathbb{R}^{H \times W \times 3}$ , and then provide the hierarchical data clustering process for constructing a multi-granularity degradation set and MoE restoration model. In Sec. 3.3, we introduce granularity estimation and how to adopt both degradation and granularity estimation for adaptive routing.

### 3.1. Preliminaries

**Mixture-of-Experts** [22, 36, 65, 68, 72, 113] is a promising way for scaling up and deploying large or gigantic models due to its competitive computational bounds and latency compared to the vanilla single model. Expert network set  $\{\mathcal{F}\}$  and routing network  $\mathcal{G}(\cdot)$  are two basic components of MoE architecture. The expert network can be a sub-layer or a sub-network (*e.g.*, convolution layer or feed-forward layer), and it also can be an independently trained network. Given input  $\mathbf{X}$ , the routing network  $\mathcal{G}(\cdot)$  is used to calculate the contribution of each expert to the final output,

$$y = \sum_{i=0}^N \mathcal{G}(h) \cdot \mathcal{F}_i(\mathbf{X}), \quad (1)$$

where  $h$  is commonly a type of representation of input  $\mathbf{X}$  which the routing network can assign expert conditioning

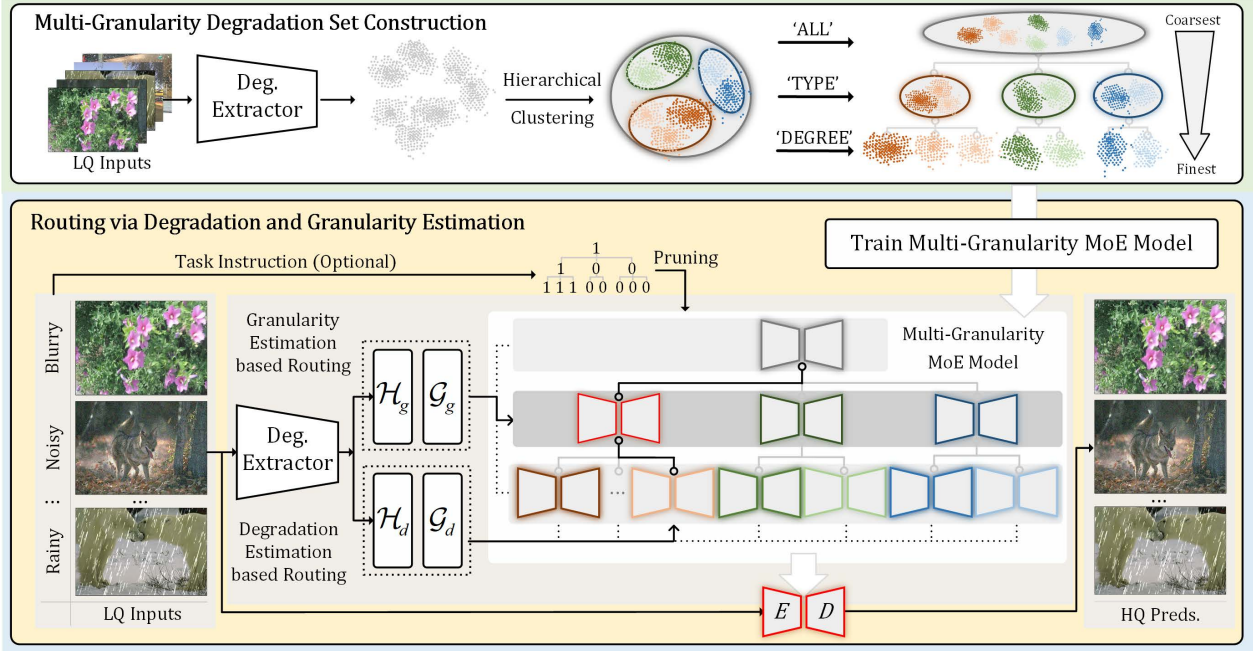


Figure 3. **Illustration of our proposed UniRestorer.** We develop a multi-granularity degradation set by hierarchical clustering on extracted DRs at different granularity, *i.e.*, ‘ALL’, ‘TYPE’, and ‘DEGREE’. Based on the multi-granularity degradation set, we train a multi-granularity MoE restoration model. Besides vanilla degradation estimation, we introduce granularity estimation to indicate the degree of degradation estimation error. Adopting both degradation and granularity estimation, we train routers to adaptively allocate an expert to unknown corrupted input.

on. The routing network is typically a noisy top- $k$  routing network parameterized with  $w_g$  and  $w_n$ , which models  $P(\mathcal{F}_k|h)$  as the probability of using the  $k$ -th expert  $\mathcal{F}_k$  and selects experts with top- $k$  probability to contribute to the final output. The noisy routing process can be described as follows,

$$\mathcal{G}(h) = \text{Softmax}(h \cdot w_g) + \mathcal{N}(0, 1) \text{Softplus}(h \cdot w_n), \quad (2)$$

where  $\text{Softplus}$  is the smooth approximation to the function  $\text{ReLU}$ . Then, the  $\text{TopK}(\cdot, k)$  function is used to select the experts with the largest  $k$  values according to  $\mathcal{G}(h)$ .

### 3.2. Multi-Granularity Degradation and Expert

**Fine-Grained DR Extractor.** Considering the convenience of using text to represent the type of degradation on corrupted images, we adopt a CLIP-based method, DA-CLIP [57], as our basic backbone. Using contrastive learning, DA-CLIP trains an image controller to separate different corrupted inputs. However, aiming to exploit finer-grained DRs (*i.e.*, degradation degree), it is essential to enable the DR extractor to be aware of finer-grained representation of degradation. Motivated by the above, we train a fine-grained DR extractor to fit our goal. In our experiments, we found that the estimation of degradation degree is sensitive to distortions, *e.g.*, noise can be heavily alleviated by transformations in the pre-processing of CLIP. To alleviate the effect of distortion on the original degradation,

we construct a dataset with fine-grained level degradations. In training, we first crop high-resolution clean images into  $224 \times 224$  patches and then add synthetic degradations with different types and degrees to obtain low-quality inputs. During inference, we center-crop the main body of given low-quality inputs to alleviate the influence of the resolution gap between training and inference. Following [57], we employ BLIP [41, 42] to generate captions for clean patches. Thus, the fine-grained DR  $e$  can be learned by the DR extractor  $\mathcal{D}$ , *i.e.*,

$$e = \mathcal{D}(\mathbf{X}). \quad (3)$$

When training is finished, we employ  $\mathcal{D}$  to obtain the DR set  $\{e\}$  from all training samples.

**Hierarchical Degradation Clustering.** To construct the proposed multi-granularity degradation set, we utilize an unsupervised data clustering approach [59], which is simple yet effective. The constructed degradation set is hierarchical. In  $i$ -th level of granularity, it consists of  $m$  non-overlapped DR groups, each of which is related to a data distribution, and samples drawn from one distribution are with similar DRs. In our implementation, we construct a hierarchical degradation set with three levels. The  $i$ -th level corresponds to a granularity  $\mathcal{C}_i$ . The coarsest level is 0-th level and the finest level is 2-th level. We first conduct data clustering at the finest-grained level by,

$$\{u\}_n \leftarrow \text{K-means}(\{e\}), \quad (4)$$

where  $\{u\}_n$  is the set of cluster centers of the finest-grained level. Based on  $\{u\}_n$ , we further conduct clustering in coarser-grained levels until the coarsest level, ‘ALL’. As a result, we obtain sets of cluster centers of our multi-granularity degradation set in coarse-to-fine level, *i.e.*  $\{u\}_0, \{u\}_1, \{u\}_2$ . Then, in the  $i$ -th level, we use function  $\operatorname{argmin}_{u_{i,j} \in \{u\}_i} (\|e - u_{i,j}\|_2^2)$  to decide which group  $\{e\}_{i,j}$  the samples belong to, and thus we can prepare training samples for the expert restoration model  $\mathcal{F}_{i,j}$ .

**Multi-Granularity MoE Restoration Model.** We train one multi-granularity MoE restoration model based on obtained multi-granularity degradation set. Expert networks are trained with  $\ell_1$  loss as the reconstruction loss between predicted results  $\hat{\mathbf{Y}}$  and target  $\mathbf{Y}$ , *i.e.*,

$$\ell_1 = \|\hat{\mathbf{Y}} - \mathbf{Y}\|_1. \quad (5)$$

It makes sense that, experts trained at coarser-grained levels can generalize to a large range of degradations, and experts trained in finer-grained levels can highly improve the restoration performance on degradations which they are good at. Therefore, given corrupted inputs, we can route them to the most appropriate expert based on an accurate degradation estimation.

### 3.3. Routing via Degradation and Granularity Est.

DR  $e$  can be regarded as routing condition  $h$  in Eq. (1). However, degradation estimation is error-prone, which may lead to inaccurate routing and thus impede restoration performance. To this end, based on the constructed multi-granularity degradation set, we estimate image degradation at the proper granularity level, and perform routing based on both degradation and granularity estimation, which makes our method robust to degradation estimation error. We train two separate branches ( $\mathcal{H}_d$  and  $\mathcal{H}_g$ ) upon  $\mathcal{D}$  for degradation estimation vector  $e_{deg}$  at the finest-grained level and granularity estimation vector  $e_{gran}$ . Then, we further train two routers  $\mathcal{G}_d(\cdot)$  and  $\mathcal{G}_g(\cdot)$  as Eq. (2) based on degradation and granularity estimation, respectively. The routing process can be described as follows,

$$\begin{aligned} \mathcal{F}_{n,k} &= \operatorname{TopK}(\mathcal{G}_d(e_{deg})|\{\mathcal{F}\}_n) \\ \mathcal{F}_{i,j} &= \operatorname{TopK}(\mathcal{G}_g(e_{gran})|\{\mathcal{F}_{0,0}, \dots, \mathcal{F}_{n,k}\}). \end{aligned} \quad (6)$$

$\mathcal{G}_d$  is conducted in the finest-grained level. Based on its routing result, it further selects a set of experts that can solve degradations belonging to  $\{e\}_{n,k}$  and are trained in different granularity levels from 0 to  $n$ . Furthermore,  $\mathcal{G}_g$  is responsible for selecting an expert training in the proper granularity according to granularity estimation.

Inspired by data uncertainty learning [13], we learn  $e_{deg}$  and  $e_{gran}$  by introducing loss as,

$$\mathcal{L}_{dg} = \frac{1}{2e_{gran}}(u_{y_i} - e_{deg})^2 + \frac{1}{2} \ln e_{gran}, \quad (7)$$

where  $u_{y_i}$  is the weight center in the finest-grained level ob-

tained by Eq. (4). We use the first term to build the relationships of  $e_{deg}$  and  $e_{gran}$ , when the distance between point estimation and predicted weight center is high, a larger  $e_{gran}$  is used to ensure that  $\mathcal{L}_{dg}$  is not too high. Therefore, the granularity can be seen as the degree of the current degradation estimation error. If estimated with a large error, granularity estimation will allocate a coarser-grained expert; Conversely, if degradation estimation is precise, granularity estimation will allocate a finer-grained expert. Thus, conditioning on both  $e_{deg}$  and  $e_{gran}$ , we can dynamically allocate given corrupted inputs with the most appropriate expert. For stable training, and to avoid the result of  $\mathcal{G}_g$  collapse to the finest-grained level, we further adopt load-balance loss as used in [72],

$$\mathcal{L}_{load} = \sigma/\mu, \quad (8)$$

where  $\mu$  and  $\sigma$  are mean and standard deviation of experts load, respectively. At last, we train our routers by jointly adopting loss as,

$$\mathcal{L}_{total} = \ell_1 + \alpha\mathcal{L}_{dg} + \beta\mathcal{L}_{load}, \quad (9)$$

where  $\alpha$  and  $\beta$  are two hyper-parameters to trade-off the effect of  $\mathcal{L}_{dg}$  and  $\mathcal{L}_{load}$ .

Typically, our framework automatically conducts the processing pipeline of extraction-recognition-routing-restoration (*auto* mode). When users are convinced about the type of degradation, we provide options that users can provide the type of degradation to instruct the routing process (*instruction* mode), as shown in Fig. 3. The instruction plays the role of pruning, it utilizes a set of masks to prune the corresponding DR groups from the multi-granularity degradation set, leading to a more efficient and accurate routing.

## 4. Experiments

### 4.1. Experimental Setup

**Datasets.** We train and evaluate our framework on two all-in-one image restoration settings: **(1) Single-Degradation:** we train a universal model to solve 7 image restoration tasks, including deraining (‘R’), dehazing (‘H’), Gaussian color denoising (‘N’), single-image motion deblurring (‘B’), low-light enhancement (‘LL’), densowing (‘S’), and compression artifacts removal (‘J’). We collect data of every included image restoration task and adopt the concatenation of the collected data as training data. Following [64, 97], We evaluate our method on Rain100L [92] for deraining, SOTS [38] for dehazing, BSD68 [58] for Gaussian color denoising, GoPro [61] for motion deblurring, LOLv1 [83] for low-light enhancement, Snow100K-L [55] for desnowing, and LIVE1 [73] for compression artifacts removal. **(2) Mixed-Degradation:** we develop our experiments in a much wider degradation, including 6 types of degradations used in single-degradation, and we evaluate 7 chal-

Table 1. **All-in-One image restoration (single-degradation) results.** We train task-agnostic models and our method on the concatenation of all restoration training data. The performance of other methods is referred from [19].  $n$ ‘D’ means  $n$ -degradation combination. PSNR and SSIM scores are calculated on RGB-channels, except scores of Rain100L are calculated on YCbCr-channels.

Methods	Derain		Dehaze		Denoise		Deblur		Lowlight		Desnow		CAR		Average		
	Rain100L[92]		SOTS[38]		BSD68[58]		GoPro[61]		LOLv1[83]		Snow100K[55]		LIVE1[73]		3D	5D	7D
	PSNR	SSIM	PSNR	PSNR	PSNR												
MPRNet [94]	26.96	0.838	16.37	0.806	23.92	0.702	25.40	0.858	7.75	0.124	19.33	0.740	27.77	0.889	18.72	22.76	19.67
SwinIR [46]	22.88	0.779	15.94	0.775	24.12	0.780	16.86	0.735	13.80	0.409	18.60	0.718	15.61	0.746	17.81	17.18	18.46
NAFNet [15]	32.79	0.942	22.43	0.907	30.27	0.918	26.53	0.877	<u>23.09</u>	0.796	26.33	0.889	<b>31.26</b>	<b>0.946</b>	24.77	25.84	26.49
Restormer [95]	35.71	0.966	29.64	0.971	31.00	<u>0.929</u>	27.50	<u>0.896</u>	22.80	0.821	<u>28.24</u>	<u>0.914</u>	<u>31.21</u>	<u>0.946</u>	30.68	28.64	<u>28.28</u>
DL [21]	32.62	0.931	26.92	0.391	30.12	0.838	-	-	-	-	-	-	-	-	28.09	-	-
AirNet [39]	34.90	0.967	27.94	0.962	31.06	0.872	-	-	-	-	-	-	-	-	29.29	-	-
PromptIR [64]	36.37	0.972	<u>30.58</u>	<u>0.974</u>	31.12	0.873	-	-	-	-	-	-	-	-	<u>31.50</u>	-	-
InstructIR-3D [19]	<u>37.98</u>	<u>0.978</u>	30.22	0.959	31.32	0.875	-	-	-	-	-	-	-	-	31.49	-	-
DL [21]	21.96	0.762	20.54	0.826	23.09	0.745	19.86	0.672	19.83	0.712	-	-	-	-	21.02	20.28	-
Transweather [79]	29.43	0.905	21.32	0.885	29.00	0.841	25.12	0.757	21.21	0.792	-	-	-	-	23.31	24.41	-
TAPE [50]	29.67	0.904	22.16	0.861	30.18	0.855	24.47	0.763	18.97	0.621	-	-	-	-	24.10	24.28	-
AirNet [39]	32.98	0.951	21.04	0.884	30.91	0.882	24.35	0.781	18.18	0.735	-	-	-	-	23.82	24.10	-
IDR [97]	35.65	0.965	25.20	0.938	31.09	0.883	26.65	0.810	20.70	0.820	-	-	-	-	27.36	26.86	-
InstructIR-5D [19]	36.84	0.973	27.10	0.956	<u>31.40</u>	0.887	<u>29.40</u>	0.886	23.00	<u>0.836</u>	-	-	-	-	28.99	<u>29.19</u>	-
Ours	<b>43.03</b>	<b>0.991</b>	<b>36.44</b>	<b>0.984</b>	<b>31.43</b>	<b>0.936</b>	<b>31.48</b>	<b>0.948</b>	<b>26.67</b>	<b>0.863</b>	<b>31.12</b>	<b>0.940</b>	30.57	0.926	<b>36.92</b>	<b>33.46</b>	<b>31.35</b>

Table 2. **All-in-One image restoration (mixed-degradation) results.** We train task-agnostic methods on synthetic mixed degradation datasets based on DF2K. The performance is evaluated on DIV2K-valid with *in-dist.* and *out-dist.* degradation parameters. ‘ $n$ T’ means  $n$ -task combination (3T: H-R, H-N, H-N-R; 5T: H-R, H-N, H-N-R, LL-H-N-R, LL-H-N-B-R; 7T: all). PSNR and SSIM scores are calculated on RGB-channels.

Methods	H-R		H-N		H-N-R		LL-H-N-R		LL-H-N-S		LL-H-N-B-R		LL-H-N-B-S		Average		
	PSNR	SSIM	3T	5T	7T												
																	PSNR
<i>In-distribution</i>																	
MPRNet [94]	17.22	0.691	19.02	0.717	17.18	0.639	17.25	0.549	17.18	0.583	16.99	0.466	<u>16.80</u>	0.506	17.80	17.57	17.37
SwinIR [46]	16.35	0.620	18.74	0.693	16.48	0.585	16.78	0.513	16.73	0.555	16.54	0.434	16.10	0.482	17.19	17.01	16.81
NAFNet [15]	19.14	0.775	22.71	0.843	18.56	0.723	17.41	0.603	17.09	0.631	16.37	0.505	15.83	<u>0.530</u>	20.13	18.98	18.15
Restormer [95]	19.85	0.795	20.44	0.820	17.64	0.719	16.86	0.588	16.56	0.623	15.92	0.483	15.47	0.520	19.31	18.27	17.53
AirNet [39]	18.67	0.752	23.34	0.855	19.03	0.726	-	-	-	-	-	-	-	-	20.34	-	-
PromptIR [79]	22.20	0.825	24.23	<b>0.886</b>	20.86	0.772	-	-	-	-	-	-	-	-	22.43	-	-
MiOIR [87]	<u>24.58</u>	<u>0.892</u>	<u>24.46</u>	0.879	<u>22.42</u>	<u>0.818</u>	<u>19.46</u>	0.661	-	-	<u>18.12</u>	0.561	-	-	<u>23.82</u>	<u>21.80</u>	-
InstructIR [19]	21.57	0.827	23.80	0.838	21.14	0.775	19.21	<u>0.666</u>	-	-	18.06	<u>0.564</u>	-	-	22.17	20.75	-
OneRestore [25]	17.35	0.711	18.70	0.669	16.41	0.617	16.66	0.621	20.24	<u>0.769</u>	-	-	-	-	17.48	-	-
Ours	<b>29.63</b>	<b>0.950</b>	<b>26.93</b>	<u>0.880</u>	<b>26.33</b>	<b>0.875</b>	<b>24.29</b>	<b>0.830</b>	<b>22.71</b>	<b>0.790</b>	<b>21.87</b>	<b>0.735</b>	<b>20.10</b>	<b>0.729</b>	<b>27.63</b>	<b>25.81</b>	<b>24.55</b>
<i>Out-of-distribution</i>																	
MPRNet [94]	15.71	0.636	16.38	0.598	15.57	0.560	14.84	0.345	14.59	0.355	14.58	0.286	<u>14.33</u>	0.299	15.88	15.41	15.14
SwinIR [46]	15.10	0.556	15.79	0.553	14.50	0.486	14.72	0.341	14.32	0.353	14.29	0.282	13.95	0.298	15.13	14.88	14.66
NAFNet [15]	16.77	0.713	19.68	0.751	15.11	0.595	14.40	0.385	14.05	0.390	13.89	0.317	13.27	<u>0.324</u>	17.18	16.00	15.31
Restormer [95]	17.44	0.723	17.31	0.738	17.44	<u>0.723</u>	14.11	0.378	13.59	0.388	13.60	0.314	12.83	0.318	17.39	15.97	15.18
AirNet [39]	17.50	0.732	20.16	0.777	15.07	0.380	-	-	-	-	-	-	-	-	17.57	-	-
PromptIR [79]	19.84	0.797	20.57	0.795	18.22	0.672	-	-	-	-	-	-	-	-	19.54	-	-
MiOIR [87]	<u>20.85</u>	<u>0.850</u>	<u>22.39</u>	<u>0.821</u>	<u>18.87</u>	0.700	15.27	0.406	-	-	<u>14.70</u>	<u>0.332</u>	-	-	<u>20.70</u>	<u>18.41</u>	-
InstructIR [19]	20.33	0.825	19.02	0.636	17.74	0.597	15.34	0.386	-	-	14.52	0.296	-	-	19.03	17.39	-
OneRestore [25]	17.81	0.732	16.77	0.580	15.10	0.595	<u>17.49</u>	<u>0.566</u>	<b>21.04</b>	<b>0.682</b>	-	-	-	-	16.56	-	-
Ours	<b>27.32</b>	<b>0.937</b>	<b>23.82</b>	<b>0.811</b>	<b>23.42</b>	<b>0.801</b>	<b>20.21</b>	<b>0.661</b>	<u>20.15</u>	<u>0.631</u>	<b>17.49</b>	<b>0.529</b>	<b>18.03</b>	<b>0.543</b>	<b>24.85</b>	<b>22.45</b>	<b>21.49</b>

lenging mixed degradation settings, *e.g.*, H-R, H-N, H-N-R, LL-H-N-R, LL-H-N-S, LL-H-N-B-R, and LL-H-N-B-S. Based on high-quality clean images from DF2K [2, 48] and DIV2K-valid, we synthesize mixed degradation datasets for training and evaluation, respectively. To demonstrate the generalization ability, we conduct comparisons on real-

world degradations, including LHP [24] for real-world de-raining, LOLv2 [89] for real-world low-light enhancement, and RealSnow [55] for real-world desnowing. For mixed-degradation, we conduct comparisons on both *in-dist.* and *out-dist.* degradation parameters.

**Comparison Method Settings.** We compare our proposed

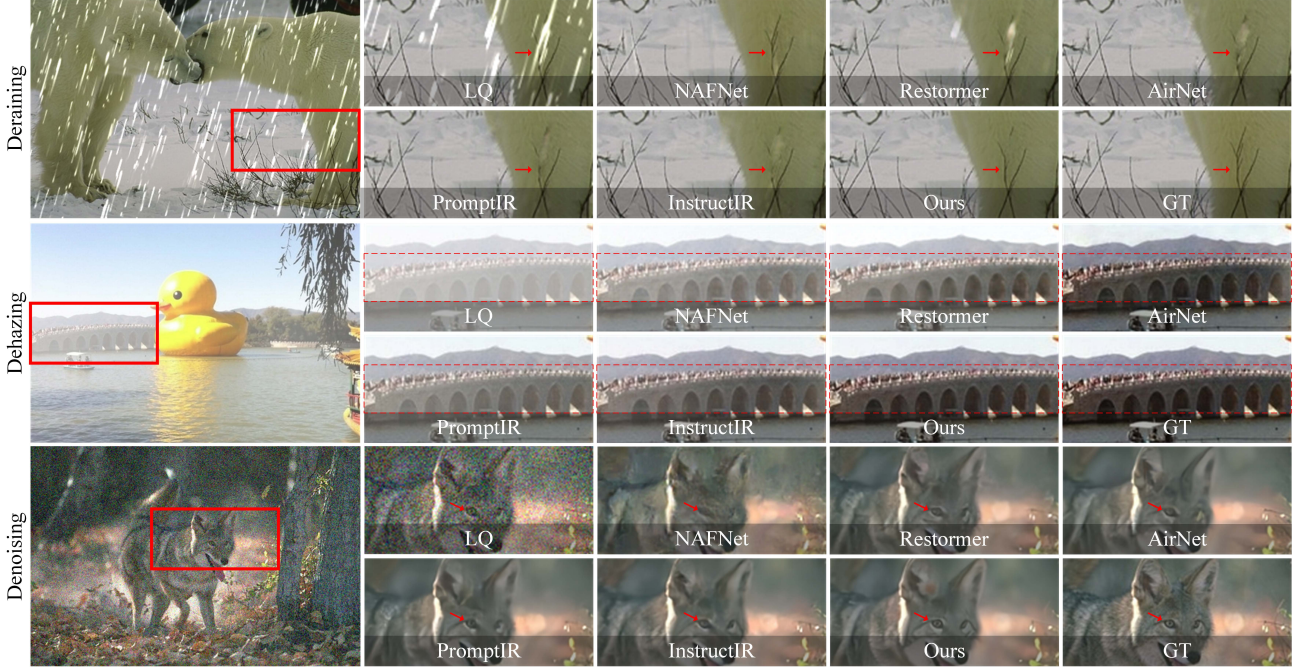


Figure 4. **Visual comparison of results on All-in-One image restoration (single-degradation).** More results can be seen in *Suppl.*

Table 3. **Compare to Single-task image restoration models.** The task-agnostic methods are trained and evaluated on single-task datasets. Our results are reported without additional single-task training. Ours and Ours<sup>†</sup> are *Auto* and *Instruction* modes, respectively. PSNR and SSIM scores are calculated on RGB-channels, except scores on deraining datasets are calculated on YCbCr-channels.

Task & Datasets		MPRNet [94]		SwinIR [46]		Restormer [95]		NAFNet [15]		Ours <sup>†</sup>	
		PSNR	SSIM	PSNR	SSIM	PSNR	SSIM	PSNR	SSIM	PSNR	SSIM
<b>Derain</b>	Rain200H [92]	<u>31.53</u>	<b>0.943</b>	29.69	0.893	30.98	0.912	29.08	0.896	<b>32.01</b>	<u>0.932</u>
	Rain200L [92]	35.92	0.966	38.35	0.981	<u>40.33</u>	0.986	38.93	<u>0.983</u>	<b>41.61</b>	<b>0.989</b>
	Test1200 [96]	<u>35.34</u>	<u>0.943</u>	34.51	0.934	35.26	0.942	35.21	0.941	<b>35.50</b>	<b>0.945</b>
	Test2800 [23]	<u>34.19</u>	<u>0.944</u>	33.26	0.934	34.16	0.943	32.84	0.932	<b>34.40</b>	<b>0.946</b>
<b>Gaussian Denoising</b> on Urban100 [62]	$\sigma=15$	34.91	0.978	34.81	0.973	<u>34.92</u>	<u>0.973</u>	34.80	0.973	<b>35.00</b>	<b>0.974</b>
	$\sigma=25$	32.67	0.959	32.51	0.958	<u>32.70</u>	<u>0.960</u>	32.58	0.959	<b>32.75</b>	<b>0.961</b>
	$\sigma=50$	29.62	0.929	29.29	0.924	<u>29.70</u>	<b>0.931</b>	29.50	0.930	<b>29.75</b>	<b>0.931</b>
<b>Desnowing</b> on Snow100K [55]	Small	36.22	0.973	33.45	0.960	<u>36.50</u>	<u>0.973</u>	35.94	0.970	<b>36.94</b>	<b>0.974</b>
	Medium	34.49	<u>0.967</u>	32.00	0.952	<u>34.77</u>	<u>0.967</u>	33.95	0.961	<b>35.18</b>	<b>0.969</b>
	Large	30.63	<u>0.938</u>	28.40	0.915	<u>30.86</u>	<u>0.938</u>	29.50	0.924	<b>31.14</b>	<b>0.940</b>
<b>CAR</b> on LIVE1 [73]	$q=10$	27.87	0.877	26.16	0.828	27.89	0.878	<b>27.95</b>	<b>0.879</b>	<u>27.94</u>	<b>0.879</b>
	$q=20$	<u>30.23</u>	0.925	28.62	0.899	30.21	0.925	30.24	<u>0.926</u>	<b>30.31</b>	<b>0.927</b>
	$q=30$	<u>31.57</u>	<u>0.943</u>	29.93	0.923	31.56	<u>0.943</u>	31.56	<u>0.943</u>	<b>31.66</b>	<b>0.944</b>
	$q=40$	<u>32.50</u>	<u>0.953</u>	30.81	0.936	32.48	<u>0.953</u>	32.47	<u>0.953</u>	<b>32.58</b>	<b>0.954</b>
<b>Low-light Enh.</b>	LOLv1 [83]	23.51	0.839	19.87	0.755	23.66	0.848	<u>23.75</u>	<u>0.855</u>	<b>27.25</b>	<b>0.864</b>
<b>Motion-Deblur</b>	GoPro [61]	32.66	0.959	29.09	0.916	32.92	0.961	<u>33.69</u>	<u>0.967</u>	<b>33.71</b>	<b>0.967</b>
<b>Dehaze</b>	SOTS-outdoor [38]	31.07	0.980	28.35	0.968	<u>33.18</u>	<u>0.984</u>	22.70	0.910	<b>37.45</b>	<b>0.992</b>
<b>Average</b>		31.22	0.939	29.07	0.913	<u>31.65</u>	<u>0.941</u>	30.00	0.930	<b>33.02</b>	<b>0.945</b>

method with task-agnostic methods [15, 46, 94, 95] and all-in-one methods [19, 21, 25, 39, 50, 64, 79, 97]. We re-train each task-agnostic method with the same experimental settings as ours. For previous all-in-one image restoration methods, we follow the evaluation setting of [14] and evaluate these methods only on tasks they support.

**Implementation Details.** For the training of experts, we generally use the AdamW optimizer with batch-size of 8

and patch-size of 128, we take the CosineAnnealing learning rate scheduler with the initial learning rate of  $3e^{-4}$ . After the training, the weights of experts are frozen, and we train degradation and granularity estimation based routers. For the training of routers, we adopt Adam optimizer with batch-size of 8 and patch-size of 256, we adopt a fixed learning rate of  $1e^{-3}$ , and we set  $\alpha$  to 0.1 and  $\beta$  to 0.01 in Eq. (9). All experiments are trained on 8 NVIDIA A6000

Table 4. DR Extractor  $\mathcal{D}$ .

Methods	Rain	Rain	Test	Test
	200H	200L	1200	2800
VGG [75]	31.47	40.59	35.26	34.18
DDR [52]	30.97	40.37	35.25	34.17
DA-CLIP [57]	31.65	40.67	35.24	34.12
Manual div.	31.88	41.43	35.32	34.23
Ours	<b>32.01</b>	<b>41.61</b>	<b>35.50</b>	<b>34.40</b>

Table 5. Different granularity.

# DRs	MiO (Average)	
	<i>In-dist.</i>	<i>Out-dist.</i>
1	22.06	17.23
2	22.42	17.51
4	23.75	<b>18.49</b>
8	<b>24.22</b>	18.35

Table 6. Granularity estimation.

$\{C\}$	# DRs	MiO (Average)	
		<i>In-dist.</i>	<i>Out-dist.</i>
$\{C_2\}$	8	24.22	18.35
$\{C_0, C_2\}$	9	24.27	18.86
$\{C_1, C_2\}$	12	24.44	19.06
$\{C_0, C_1, C_2\}$	13	<b>24.46</b>	<b>19.45</b>

Table 7. Loss functions.

$\ell_1$	$\mathcal{L}_{dg}$	$\mathcal{L}_{load}$	MiO (Average)	
			<i>In-dist.</i>	<i>Out-dist.</i>
✓			24.14	18.37
✓	✓		24.35	18.76
✓	✓	✓	<b>24.46</b>	<b>19.45</b>

Table 8. Generalization performance on real-world datasets.

All methods are evaluated without training on corresponding training data. PSNR and SSIM scores are calculated on RGB-channels, except scores of Rain100L are calculated on YCbCr-channels.

Methods	Deraining		Low-light Enh.		Desnowing		Average	
	LHP [24]	LHP [24]	LOLv2-real [89]	LOLv2-real [89]	RealSnow [112]	RealSnow [112]	PSNR	SSIM
MPRNet [94]	30.65	0.877	9.67	0.170	25.82	0.831	28.21	0.861
SwinIR [46]	23.38	0.832	18.67	0.730	18.45	0.723	22.14	0.804
NAFNet [15]	27.53	0.838	26.46	0.861	<u>27.51</u>	<u>0.881</u>	27.44	0.847
Restormer [95]	28.71	0.856	28.92	0.898	26.73	0.875	28.37	0.862
PromptIR [64]	27.17	0.856	-	-	-	-	-	-
MiOIR [87]	30.21	0.872	10.62	0.284	-	-	-	-
InstructIR [19]	30.50	<b>0.889</b>	<u>30.31</u>	<b>0.909</b>	-	-	-	-
OneRestore [25]	26.10	0.820	17.76	0.657	20.12	0.726	24.40	0.791
Ours	<b>31.60</b>	<u>0.879</u>	<b>30.40</b>	<u>0.901</u>	<b>28.04</b>	<b>0.888</b>	<b>30.87</b>	<b>0.882</b>

GPUs. More details of the experimental setup, datasets, and implementation can be seen in *Suppl.*

## 4.2. Comparison with State-of-The-Art Methods

**Comparison with All-in-One Models.** With the increasing number of restoration tasks, it is difficult for the tailored all-in-one methods to have obvious performance gain over SOTA task-agnostic methods. Our method can significantly outperform task-agnostic and all-in-one methods by a large margin in **Setting 1** (Tab. 1 and Fig. 4). In **Setting 2**, our method continuously achieves higher performance than task-agnostic and all-in-one methods from simple to complex mixed degradation (Tab. 2). In addition, comparisons on *out-dist.* and *real-world* image restoration datasets (Tab. 8) reveal our method also guarantees better generalization performance than others. More visual comparison results of all-in-one image restoration can be seen in *Suppl.*

**Comparison with Single-Task Models.** For a fair comparison, we evaluate the performance of our method under *instruction* mode (Ours<sup>†</sup>). As shown in Fig. 3, each task instruction corresponds to a binary mask. Based on the mask, we prune out the unrelated expert models, leaving the corresponding experts as a sub-model of the original trained multi-granularity MoE model. We then allocate experts based on degradation and granularity estimation for given corrupted inputs. As shown in Tab. 3, by learning image degradation in finer granularity, and utilizing pruning to alleviate degradation estimation error, our method can outperform single-task models without additional training. Implementation and visual comparisons can be seen in *Suppl.*

## 4.3. Ablation Study

**Effect of Different DR Extractors.** As shown in Tab. 4, we learn experts using data clustered by different DR extractors, including VGG [75], DDR [52], DA-CLIP [57], manually division by publicly released dataset (Manual div.), and our method. Since we learn finer-grained DR, our experts can achieve better performance than others.

**Effect of Different Granularity.** As shown in Tab. 5, with the whole degradation space grouped into more DR groups, the performance on *in-dist.* steadily improves. As for generalization performance on *out-dist.*, clustering DR groups in coarser-grained level sometimes performs better than in finer-grained levels, demonstrating that it is essential to combine multiple granularities in our method.

**Effect of Granularity Estimation.** Based on the finest-grained level  $C_2$ , we evaluate the performance of different granularity combinations. As shown in Tab. 6, with granularity estimation, incorporating both fine-grained levels and coarse-grained levels can maintain much better restoration performance and generalization ability than employing single granularity.

**Effect of  $\mathcal{L}_{dg}$  and  $\mathcal{L}_{load}$**  As shown in Tab. 7, both  $\mathcal{L}_{dg}$  and  $\mathcal{L}_{load}$  can benefit more accurate routing. In particular,  $\mathcal{L}_{dg}$  and  $\mathcal{L}_{load}$  can avoid the routing to collapse to the finest-grained level, improving performance on *out-dist.*

## 5. Conclusion

In this paper, we introduced our UniRestorer, a new universal image restoration framework aiming to leverage degradation priors to improve the restoration performance while alleviating the inevitable error in degradation estimation. We learn all-in-one image restoration in multiple granularities and propose to estimate image degradation at proper granularity. Specifically, we perform hierarchical clustering on degradation space and develop a multi-granularity degradation set as well as a MoE restoration model. Besides vanilla degradation estimation, granularity estimation is further introduced to indicate the degree of degradation estimation error. By adopting both degradation and granularity estimation, we train routers to adaptively allocate unknown corrupted inputs to the most appropriate expert. Experimental results demonstrate our superior performance and promising potential in closing the performance gap to specific single-task models.

# UniRestorer: Universal Image Restoration via Adaptively Estimating Image Degradation at Proper Granularity

## Supplementary Material

The content of the supplementary material involves:

- Degradation pipeline and parameters in Sec. A.
- Implementation Details in Sec. B.
- Overhead comparisons in Sec. C.
- More visual comparisons in Sec. D.

### A. Degradation Pipeline and Parameters

**Degradation Pipeline.** We follow the degradation pipeline of [103] to construct synthetic low-quality datasets for the training of the degradation extractor and all-in-one image restoration in mixed-degradation setup. As shown in Fig. A, given high-quality clean inputs  $y$ , we orderly add synthetic lowlight, blur, noise, rain, snow, and haze to synthesize corresponding low-quality outputs  $x$ . We adopt gates between different degradations to gap one of them probably, the probability of all gates is generally set to 0.5. The way of each degradation is introduced as follows:

**Blur.** Following [99], we synthesize blurring degradation as,

$$x = y \otimes k, \quad (\text{A})$$

where  $k$  is the blur kernel. In our implementation, the type of blur kernel includes isotropic and anisotropic, each of which is employed with the probability of 0.5. The kernel size is sampled in the range from 7 to 23. The standard deviation of the Gaussian kernel is set from 1 to 3 for *in-dist.* and 3 to 4 for *out-dist.*

**Noise.** Gaussian noise is synthesized as,

$$x = y + n, \quad (\text{B})$$

where  $n$  is Gaussian noise with variance  $\sigma^2$ .  $\sigma$  is set from 15 to 35 for *in-dist.* and 35 to 50 for *out-dist.*

**Rain.** Raining degradation is synthesized as,

$$x = y + r, \quad (\text{C})$$

where  $r$  is rain streaks. Following [87],  $r$  is synthesized with random noise and Gaussian blur, where noise is related to the strength of the rain, and blur kernel is related to the rain direction, length, and width. We adopt the number of rain streaks from 50 to 100 in *in-dist.* and 100 to 150 for *out-dist.* Rain direction is generally adopted from  $-45^\circ$  to  $45^\circ$ , rain length is set from 20 to 40, and rain width is uniformly sampled from  $\{3, 5, 7, 9, 11\}$ .

**Haze.** Following [38], hazing degradation is synthesized as,

$$\begin{aligned} x &= T(y)y + a(1 - T(y)), \\ T(y) &= e^{-\beta D(y)}, \end{aligned} \quad (\text{D})$$

where  $a$  is the global atmospheric light,  $T(y)$  is the transition matrix,  $D(y)$  is the depth map, and  $\beta$  is the scattering coefficient of the atmosphere. In haze degradation synthesizing, the value of  $\beta$  largely decides the thickness of haze. We adopt one publicly released project MegaDepth<sup>1</sup> to estimate the depth image. In our experiments, the global atmospheric light is set from 0.8 to 1, the  $\beta$  is set from 0.5 to 1.5 for *in-dist.* and 1.5 to 2 for *out-dist.*

**Snow.** Snowing degradation is synthesized as,

$$x = y \times (1 - m) + m, \quad (\text{E})$$

where  $m$  is the snow mask randomly sampled from Snow100K [55] dataset.

**Lowlight.** Following [25], lowlight degradation is synthesized as,

$$x = \frac{y}{I(y)} I(y)^\gamma \quad (\text{F})$$

where  $I(y)$  is the illusion map obtained from RetinexFormer [10] and  $\gamma$  is the darkening coefficient. Since we explicitly include noise degradation in our degradation pipeline, we do not additionally consider noise in this step. We set  $\gamma$  from 1 to 2 for *in-dist.* and 2 to 2.5 for *out-dist.*

Besides, JPEG compression is synthesized by employing the publicly released project DiffJPEG<sup>2</sup>.

**Degradation representation extractor.** To train our degradation representation (DR) extractor, we adopt the above ways to synthesize various types of low-quality data. According to the parameter that decides the degradation degree, we separate synthetic data into multiple groups. For deraining degradation, strength from 0 to 50 is small rain, 50 to 100 is medium rain, and 100 to 150 is large rain; In denoising,  $\sigma$  of Gaussian noise from 0 to 15 is small noise, 15 to 35 is medium noise, and 35 to 50 is large noise; In dehazing, scattering coefficient  $\beta$  larger than 0.1 is thick haze,  $\beta$  smaller than 0.1 is normal haze; In deblurring, kernel size of motion blur kernel larger than 15 is large blur, kernel size smaller than 15 is small blur; In desnowing, we use snow masks from Snow100K dataset and adopt the official separation. In compression artifacts removal, image quality from 0 to 15 is large compression, 15 to 35 is medium

<sup>1</sup><https://github.com/zhengqili/MegaDepth>

<sup>2</sup><https://github.com/mlomnitz/DiffJPEG>

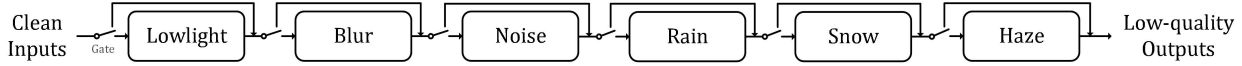


Figure A. Degradation Pipeline.

compression, 35 to 50 is small compression; In lowlight enhancement, the darkening coefficient from 1 to 1.5 is light corruption and 1.5 to 3 is heavy corruption.

## B. Implementation Details

**Multi-Granularity MoE Restoration Model.** To construct our MoE restoration model, we adopt Restormer [95] as the expert model for most of the tasks, except for lowlight enhancement, for which we choose RetinexFormer [10] as the expert model. In single-degradation setting, we set two experts for lowlight enhancement, deblurring, and dehazing to learn to restore light corruptions and heavy corruptions, respectively. We set three experts for desnowing, denoising, and CAR to learn light corruptions, medium corruptions, and heavy corruptions, respectively. Considering the diversity of rain degradation, we adopt four experts for de-raining task. As a result, our MoE restoration model has three granularities. In the coarsest-grained level, we use one expert model to solve all observed degradations; in the second level, we use seven experts to solve different tasks; and in the finest-grained level, we totally have nineteen experts, and each expert is responsible for one specific type of degradation with specific degradation degree.

**Structure of  $\mathcal{H}$  and  $\mathcal{G}$ .** Without dedicated design, we adopt 5-layer MLP for both  $\mathcal{H}_d$  and  $\mathcal{H}_g$ , in which the number of input and output channels is 512 (the same with the dimension of DR  $e$ ). The structure of  $\mathcal{G}_d$  and  $\mathcal{G}_g$  is one-layer MLP with input channels of 512 and the number of output channels equal to the number of experts.

**Ours<sup>†</sup>.** The *instruction* mode of our method allows inference based on given task instructions, *i.e.* the task name. In our implementation, the task instructions can convert to specific binary masks, which represent pruning or not pruning on the corresponding expert model in our MoE restoration model. According to the masks, we first prune out the corresponding expert models, then we conduct degradation- and granularity-based routing to find the most appropriate expert model for corrupted inputs. In this way, the error in degradation estimation is alleviated, the routing accuracy is highly improved, and thus the restoration performance is further improved.

**Ablation Study I.** We adopt pre-trained vgg16, pre-trained ESRGAN on bicubic  $4\times$  super-resolution, and pre-trained DACLIP as DR extractors, and evaluate their effect on expert restoration model. We conduct experiments on the de-raining task. We first extract DRs for all low-quality inputs, we cluster the obtained representation into four clusters, and for each cluster of samples we train one expert. Since we

Table A. Overhead comparisons.

Methods	#FLOPs (G)	Latency (s)
Restormer [95]	1128.9	0.368
NAFNet [15]	505.5	0.186
PromptIR [64]	1266.2	0.355
OneRestore [25]	94.5	0.238
Ours	1155.8	0.484

exploit DR at a finer-grained level, the experts we trained can achieve better performance than others.

## C. Overhead Comparisons

We calculate FLOPs and latency with  $1 \times 3 \times 512 \times 512$  input, on a single NVIDIA A6000 GPU. As shown in Tab. A, thanks to mixture-of-experts, the overhead of our method is slightly higher than Restormer [95]. As a result, our method can achieve high restoration accuracy and low latency simultaneously.

## D. More Visual Comparisons

We show more visual comparison results in this section. Compared to task-agnostic methods, all-in-one methods, and specific single-task models, our method can restore more clear results with detailed textures. The single-degradation results of all-in-one image restoration comparisons can be seen in Fig. B to Fig. H. The comparison results with specific single-task models can be seen in Fig. I to Fig. N. In the evaluation of mixed degradation, since the resolution of images from DIV2K-valid is too high, limiting inference on the whole image for all methods. We first crop high-resolution images into overlapped  $512 \times 512$  crops, after inference, we inverse the cropping process and re-compose crops back to one whole image, though averaging the overlapped area, the border artifacts cannot be avoidable. Comparison result of *in-dist.* and *out-dist.* can be seen in Fig. O and Fig. P, respectively.

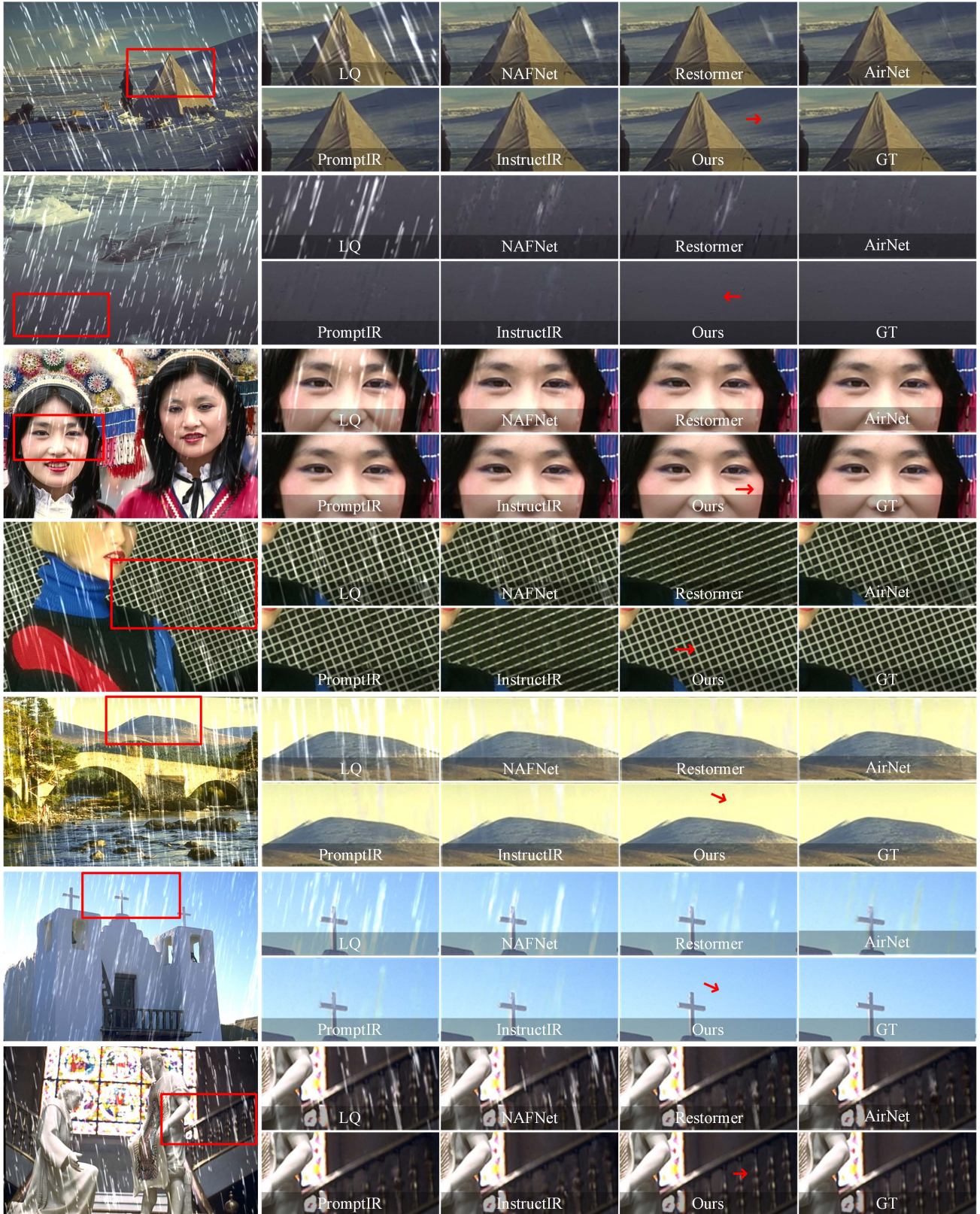


Figure B. Visual comparison of results on All-in-One image restoration (deraining).

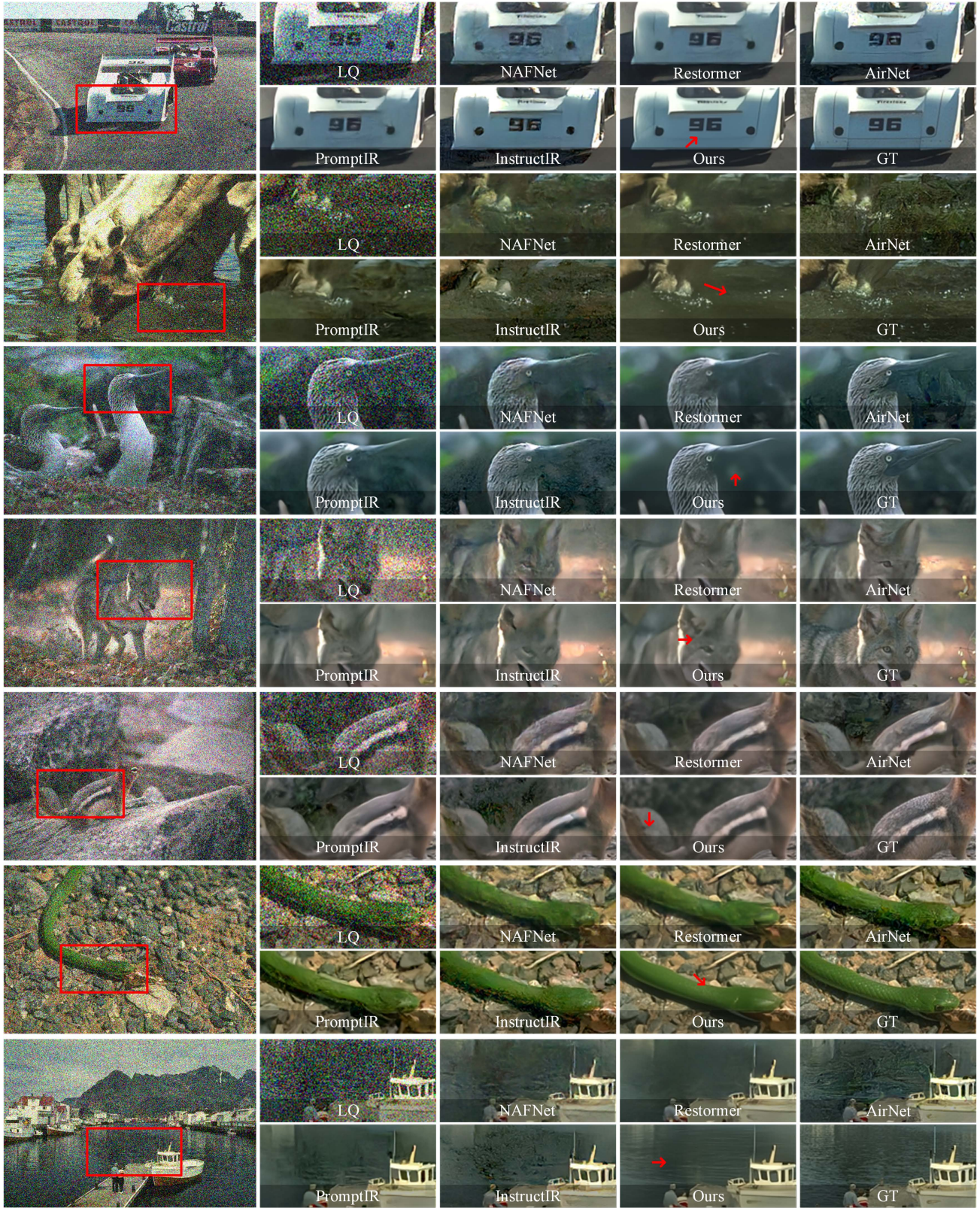


Figure C. Visual comparison of results on All-in-One image restoration (Gaussian-denoising).

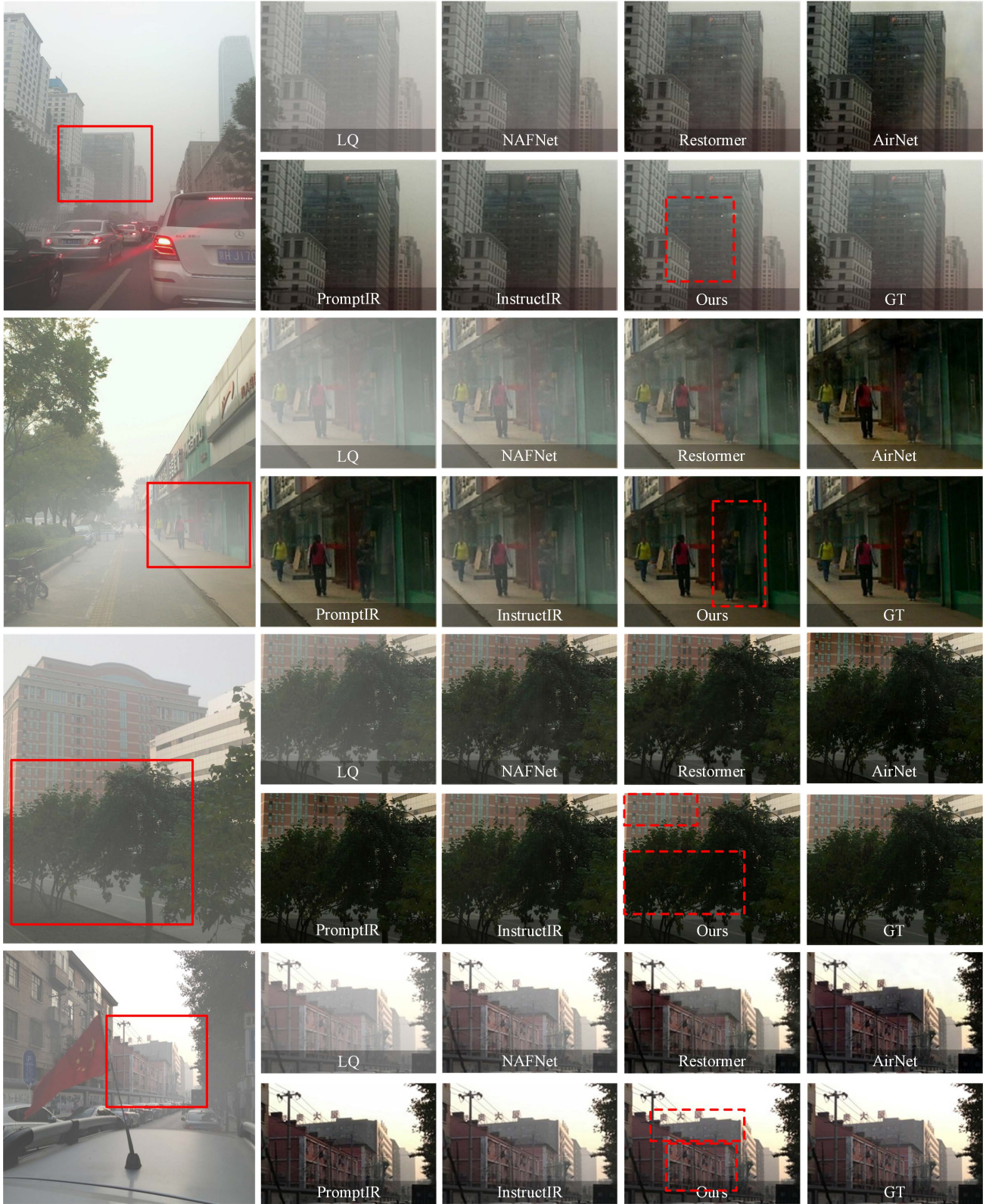


Figure D. Visual comparison of results on All-in-One image restoration (dehazing).

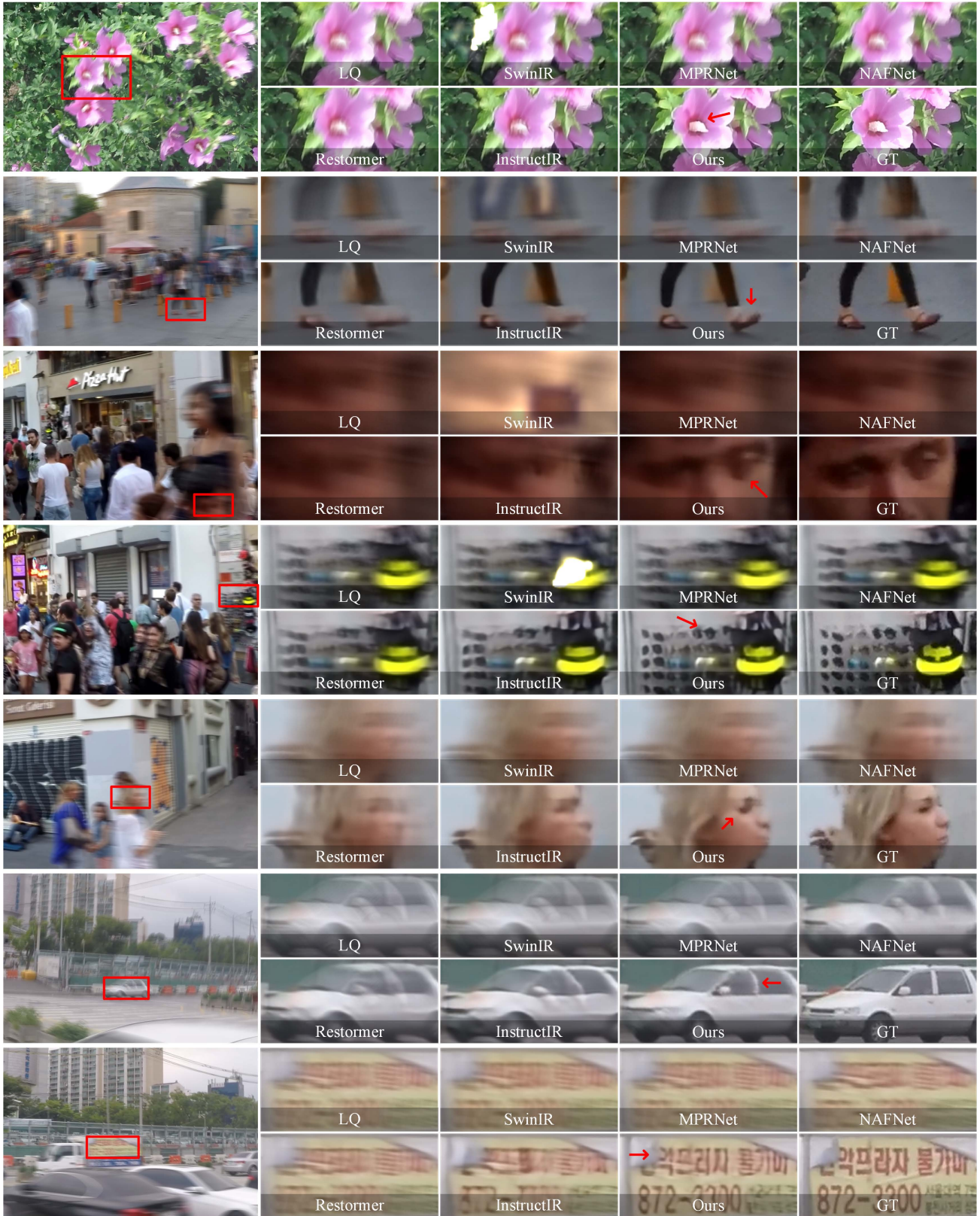


Figure E. Visual comparison of results on All-in-One image restoration (motion-deblurring).

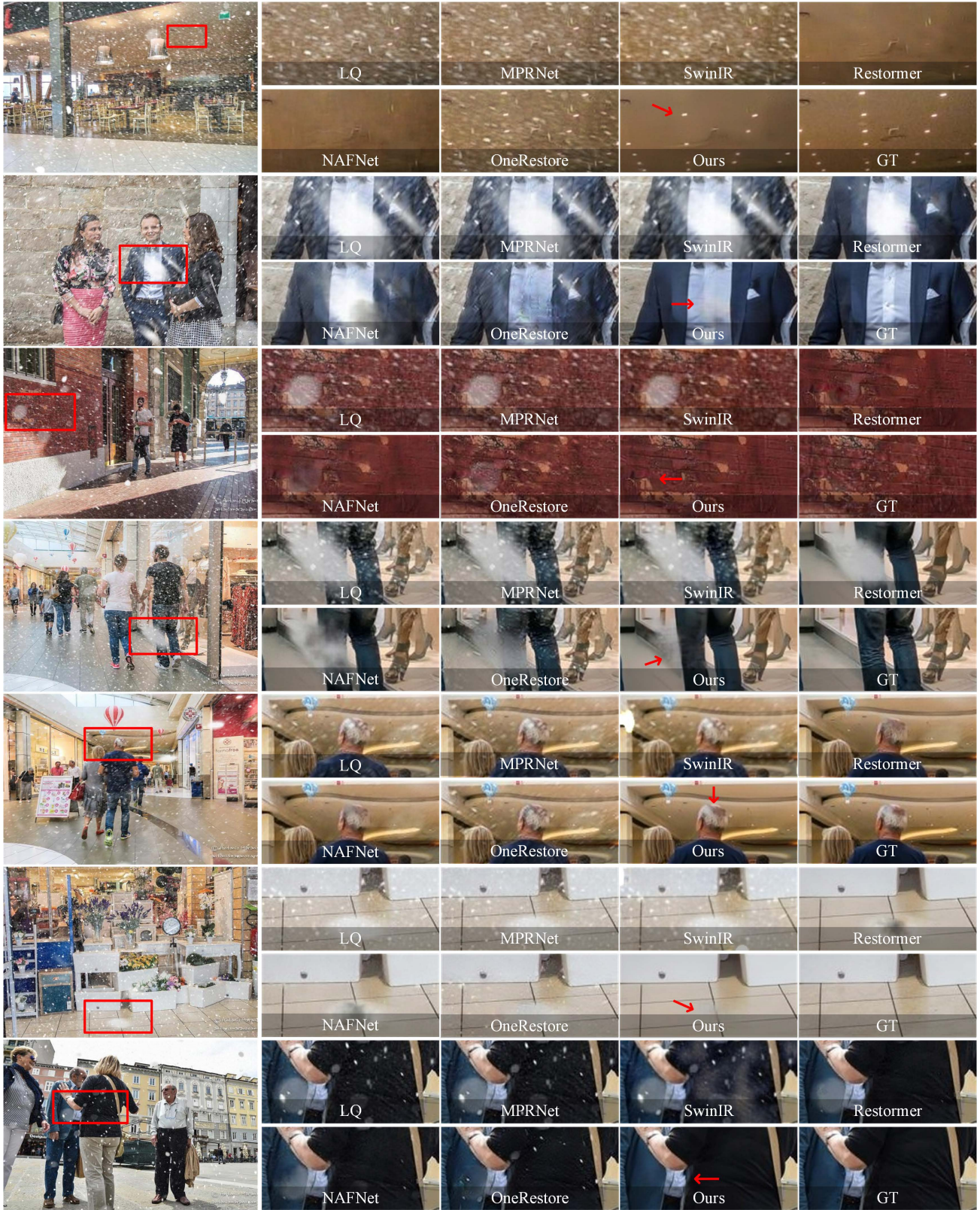


Figure F. Visual comparison of results on All-in-One image restoration (desnowing).

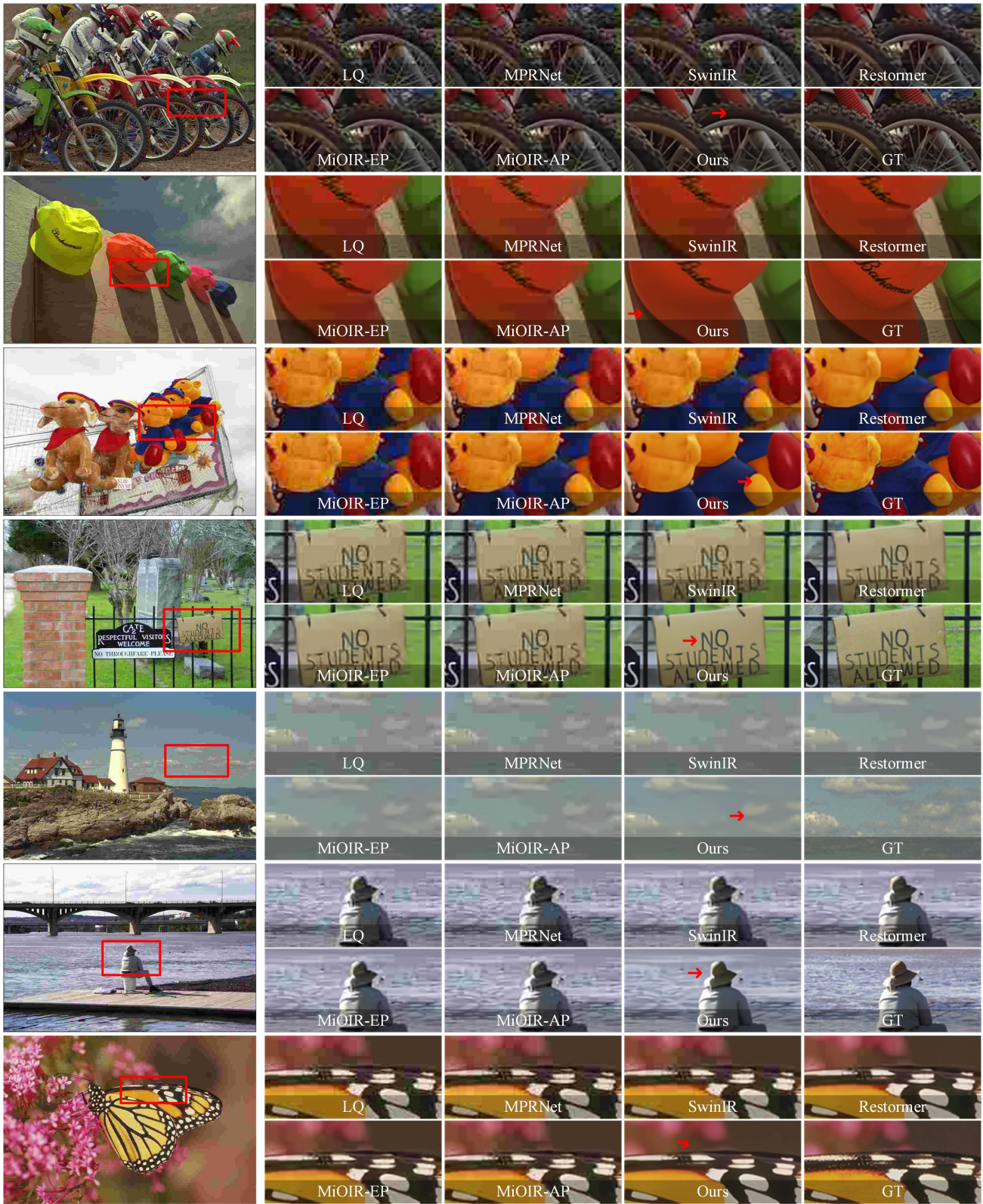


Figure G. Visual comparison of results on All-in-One image restoration (compression artifacts removal).

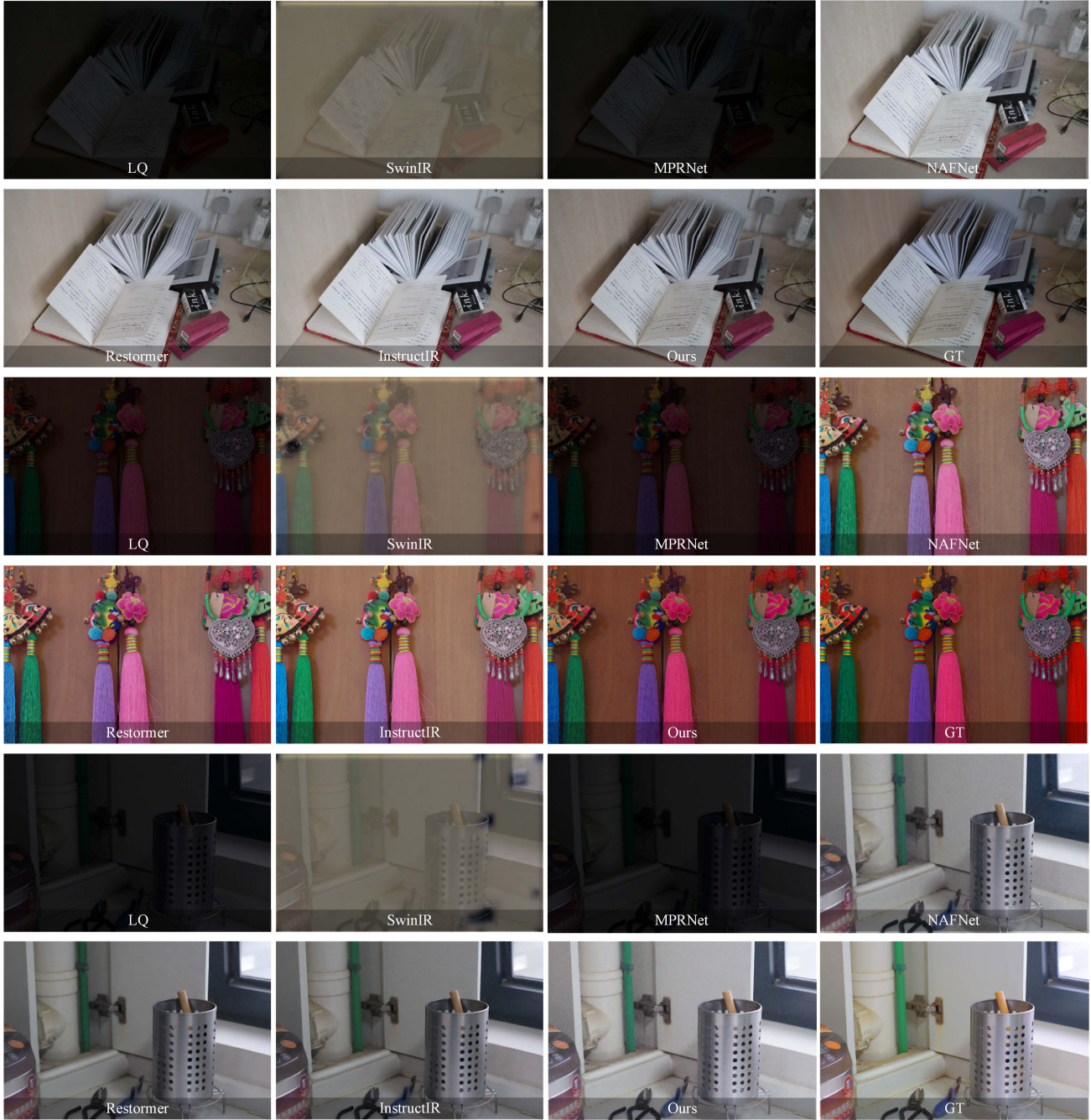


Figure H. Visual comparison of results on All-in-One image restoration (lowligh enhancement).



Figure I. Visual comparison of results with specific models (deraining).

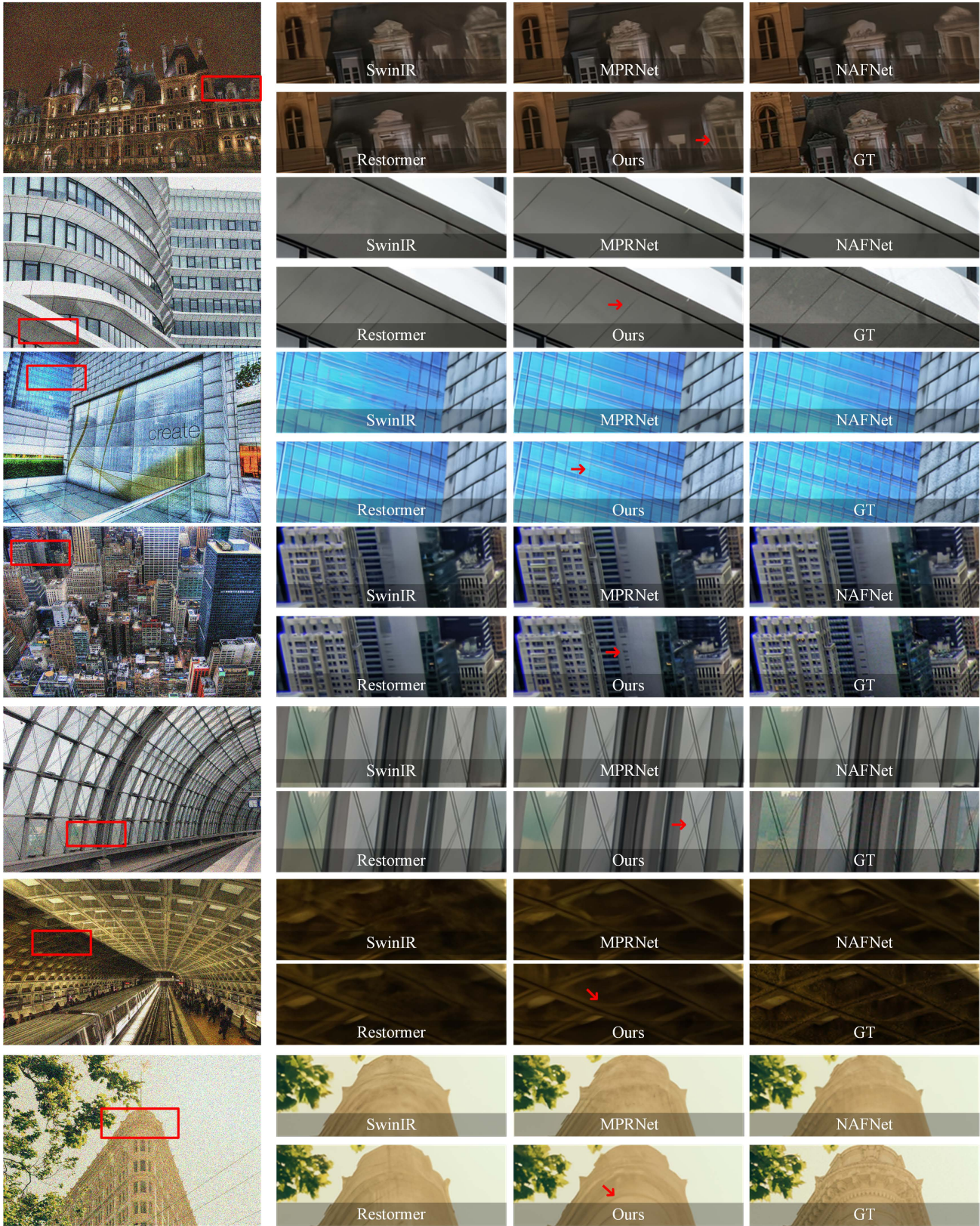


Figure J. Visual comparison of results with specific models (Gaussian-denoising).

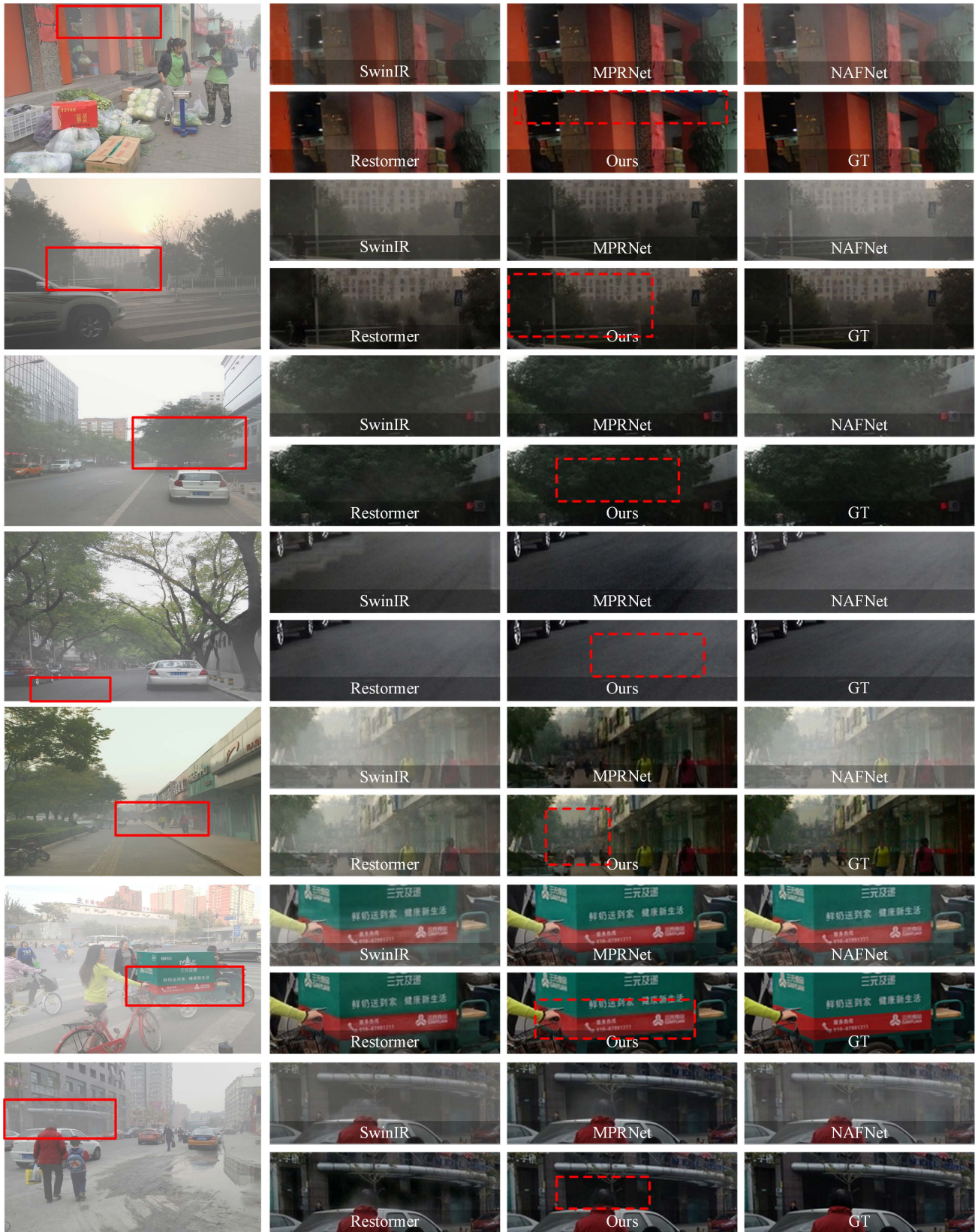


Figure K. Visual comparison of results with specific models (dehaze).

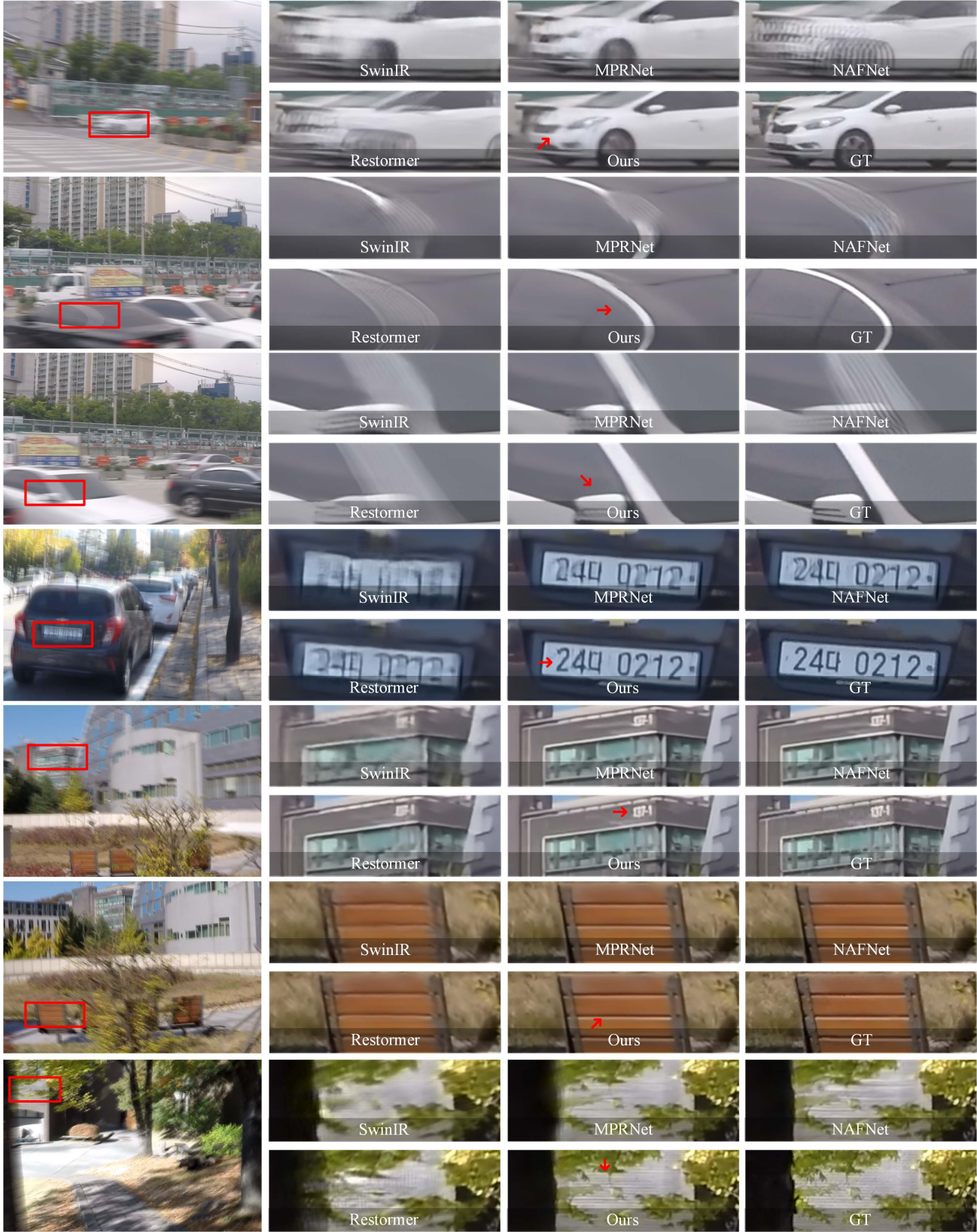


Figure L. Visual comparison of results with specific models (motion-deblurring).

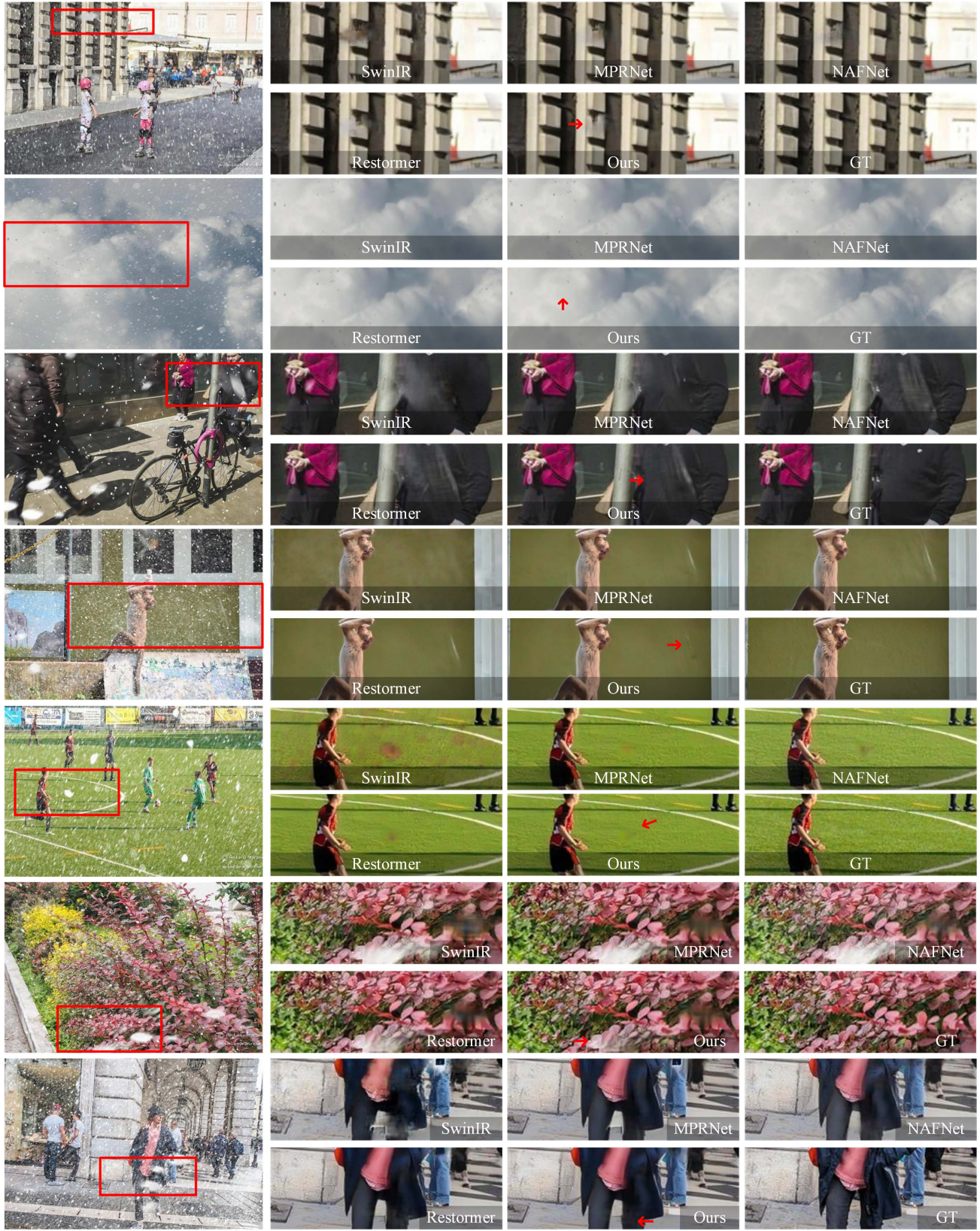


Figure M. Visual comparison of results with specific models (desnowing).

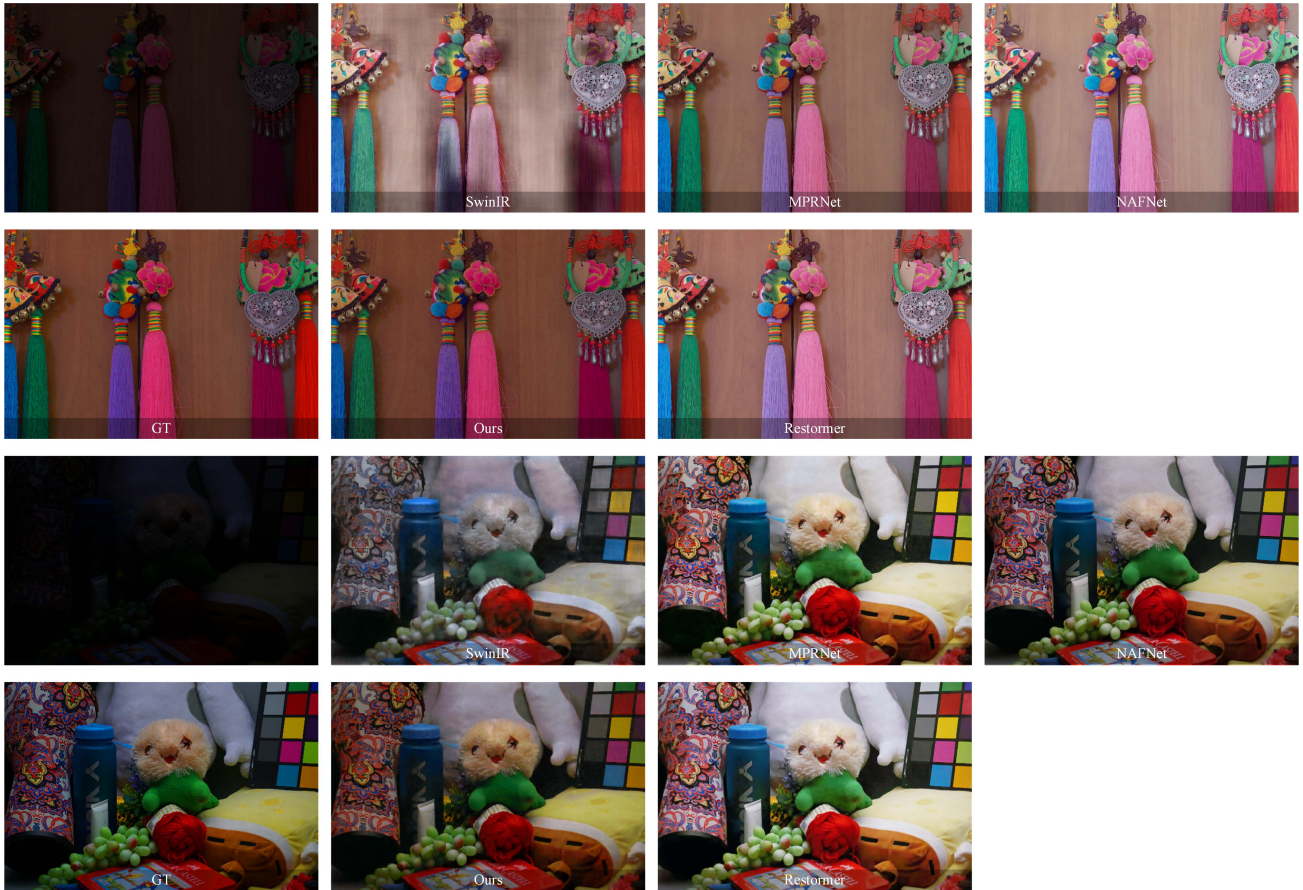


Figure N. Visual comparison of results with specific models (lowligh enhancement).

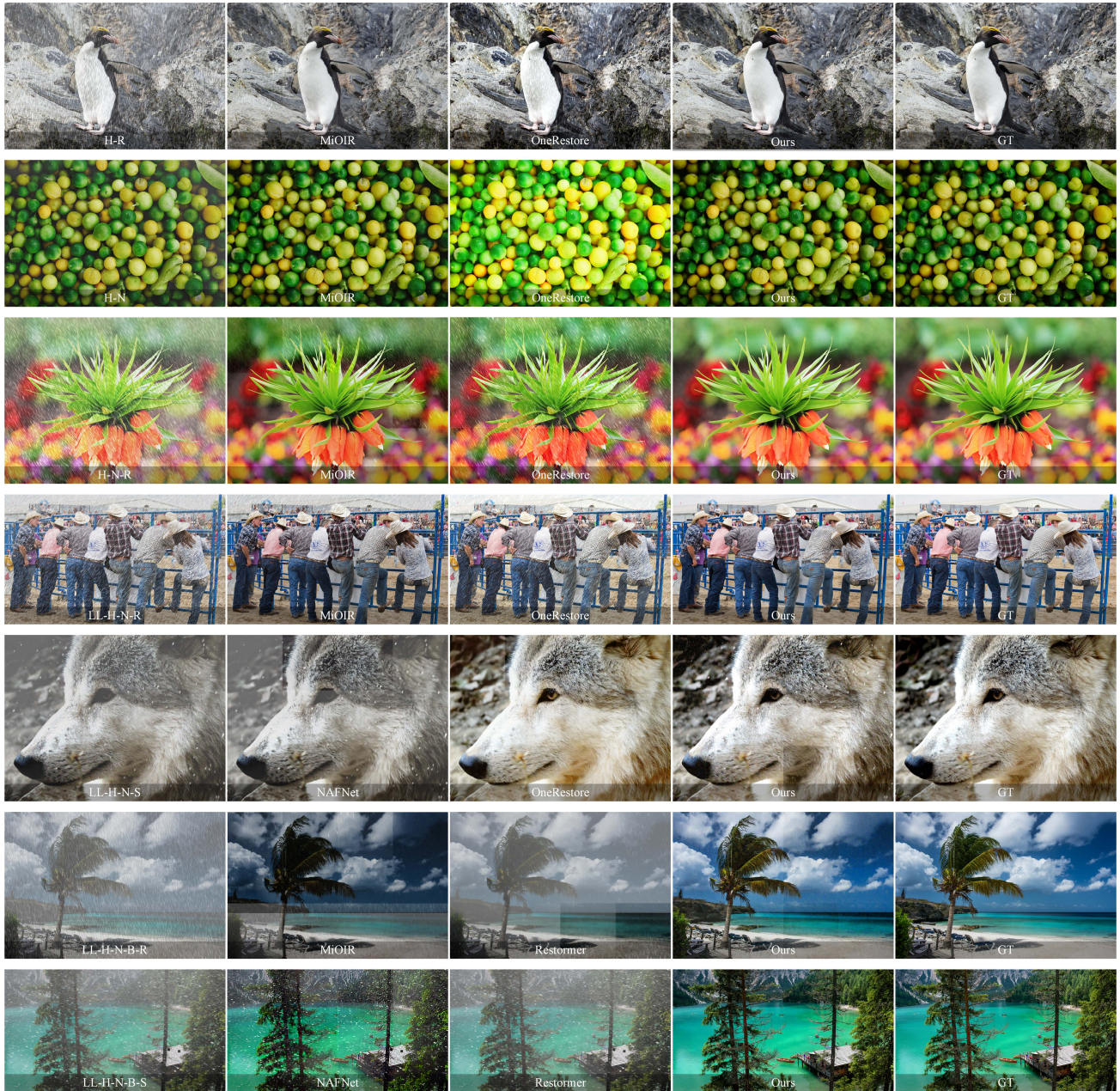


Figure O. Visual comparison of results on All-in-One image restoration (mixed-degradation, *in-dist*). Zoom in for more details.

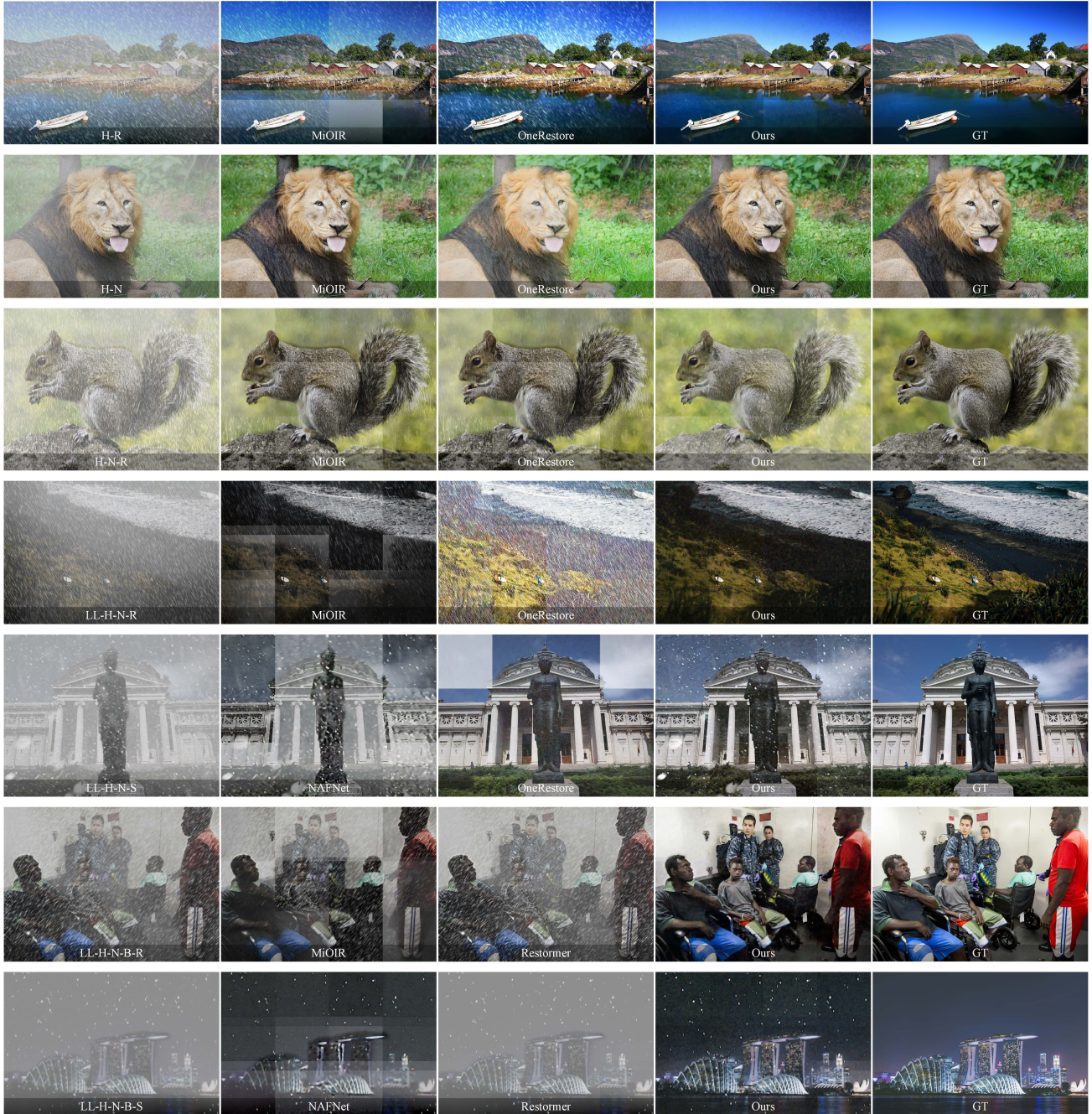


Figure P. Visual comparison of results on All-in-One image restoration (mixed-degradation, *out-dist*). Zoom in for more details.

## References

- [1] Abdelrahman Abdelhamed, Stephen Lin, and Michael S. Brown. A high-quality denoising dataset for smartphone cameras. In *CVPR*, 2018. 1
- [2] Eirikur Agustsson and Radu Timofte. Ntire 2017 challenge on single image super-resolution: Dataset and study. In *CVPRW*, 2017. 6
- [3] Yuang Ai, Huaibo Huang, and Ran He. Lora-ir: Taming low-rank experts for efficient all-in-one image restoration. *arXiv preprint arXiv:2410.15385*, 2024. 1
- [4] Yuang Ai, Huaibo Huang, Xiaoqiang Zhou, Jiexiang Wang, and Ran He. Multimodal prompt perceiver: Empower adaptiveness, generalizability and fidelity for all-in-one image restoration. In *CVPR*, 2024. 1, 3
- [5] FirstName Alpher. Frobnication. *IEEE TPAMI*, 12(1):234–778, 2002.
- [6] FirstName Alpher and FirstName Fotheringham-Smythe. Frobnication revisited. *Journal of Foo*, 13(1):234–778, 2003.
- [7] FirstName Alpher and FirstName Gamow. Can a computer frobnicate? In *CVPR*, pages 234–778, 2005.
- [8] FirstName Alpher, FirstName Fotheringham-Smythe, and FirstName Gamow. Can a machine frobnicate? *Journal of Foo*, 14(1):234–778, 2004.
- [9] Lester Brian, Al-Rfou Rami, and Constant Noah. The power of scale for parameter-efficient prompt tuning. In *EMNLP*, 2021. 1
- [10] Yuanhao Cai, Hao Bian, Jing Lin, Haoqian Wang, Radu Timofte, and Yulun Zhang. Retinexformer: One-stage retinex-based transformer for low-light image enhancement. In *ICCV*, 2023. 1, 2
- [11] Jin Cao, Yi Cao, Li Pang, Deyu Meng, and Xiaoyong Cao. Hair: Hypernetworks-based all-in-one image restoration. *arXiv preprint arXiv:2408.08091*, 2024. 1, 3
- [12] Shuo Cao, Yihao Liu, Wenlong Zhang, Yu Qiao, and Chao Dong. Grids: Grouped multiple-degradation restoration with image degradation similarity. In *ECCV*, 2024. 1, 3
- [13] Jie Chang, Zhonghao Lan, Changmao Cheng, and Yichen Wei. Data uncertainty learning in face recognition. In *CVPR*, 2020. 5
- [14] Haoyu Chen, Wenbo Li, Jinjin Gu, Jingjing Ren, Sixiang Chen, Tian Ye, Renjing Pei, Kaiwen Zhou, Fenglong Song, and Lei Zhu. Restoreagent: Autonomous image restoration agent via multimodal large language models. In *NeurIPS*, 2024. 1, 3, 7
- [15] Liangyu Chen, Xiaojie Chu, Xiangyu Zhang, and Jian Sun. Simple baselines for image restoration. In *ECCV*, 2022. 1, 3, 6, 7, 8, 2
- [16] Zitian Chen, Mingyu Ding, Yikang Shen, Wei Zhan, Masayoshi Tomizuka, Erik Learned-Miller, and Chuang Gan. An efficient general-purpose modular vision model via multi-task heterogeneous training. *arXiv preprint arXiv:2306.17165*, 2023. 3
- [17] Zitian Chen, Yikang Shen, Mingyu Ding, Zhenfang Chen, Hengshuang Zhao, Erik Learned-Miller, and Chuang Gan. Mod-squad: Designing mixtures of experts as modular multi-task learners. *CVPR*, 2023. 3
- [18] Aidan Clark, Diego de las Casas, Aurelia Guy, Arthur Mensch, Michela Paganini, Jordan Hoffmann, Bogdan Damoc, Blake Hechtman, Trevor Cai, Sebastian Borgeaud, George van den Driessche, Eliza Rutherford, Tom Hennigan, Matthew Johnson, Katie Millican, Albin Cassirer, Chris Jones, Elena Buchatskaya, David Budden, Laurent Sifre, Simon Osindero, Oriol Vinyals, Jack Rae, Erich Elsen, Koray Kavukcuoglu, and Karen Simonyan. Unified scaling laws for routed language models. In *NeurIPS*, 2022.
- [19] Marcos V. Conde, Gregor Geigle, and Radu Timofte. Instructir: High-quality image restoration following human instructions. In *ECCV*, 2024. 1, 3, 6, 7, 8
- [20] Chao Dong, Chen Change Loy, Kaiming He, and Xiaoou Tang. Learning a deep convolutional network for image super-resolution. In *ECCV*, 2014. 1, 3
- [21] Qingnan Fan, Dongdong Chen, Lu Yuan, Gang Hua, Nenghai Yu, and Baoquan Chen. A general decoupled learning framework for parameterized image operators. *IEEE TPAMI*, 2019. 6, 7
- [22] William Fedus, Barret Zoph, and Noam Shazeer. Switch transformers: Scaling to trillion parameter models with simple and efficient sparsity. *Journal of Machine Learning Research*, 2022. 3
- [23] Xueyang Fu, Jiabin Huang, Delu Zeng, Yue Huang, Xinghao Ding, and John Paisley. Removing rain from single images via a deep detail network. In *CVPR*, 2017. 1, 7
- [24] Yun Guo, Xueyao Xiao, Yi Chang, Shumin Deng, and Luxin Yan. From sky to the ground: A large-scale benchmark and simple baseline towards real rain removal. In *ICCV*, 2023. 6, 8
- [25] Yu Guo, Yuan Gao, Yuxu Lu, Ryan Wen Liu, and Shengfeng He. Onerestore: A universal restoration framework for composite degradation. In *ECCV*, 2024. 1, 6, 7, 8, 2
- [26] Jingwen He, Chao Dong, and Yu Qiao. Modulating image restoration with continual levels via adaptive feature modification layers. In *The IEEE Conference on Computer Vision and Pattern Recognition (CVPR)*, 2019.
- [27] Kaiming He, Xiangyu Zhang, Shaoqing Ren, and Jian Sun. Deep residual learning for image recognition. In *CVPR*, 2016. 1
- [28] Neil Houlsby, Andrei Giurgiu, Stanislaw Jastrzebski, Bruna Morrone, Quentin de Laroussilhe, Andrea Gesmundo, Mona Attariyan, and Sylvain Gelly. Parameter-efficient transfer learning for nlp. In *ICML*, 2019. 1
- [29] Edward J Hu, Yelong Shen, Phillip Wallis, Zeyuan Allen-Zhu, Yuanzhi Li, Shean Wang, Lu Wang, and Weizhu Chen. LoRA: Low-rank adaptation of large language models. In *ICLR*, 2022. 3
- [30] Robert A. Jacobs, Michael I. Jordan, Steven J. Nowlan, and Geoffrey E. Hinton. Adaptive mixtures of local experts. *Neural Computation*, 1991. 3
- [31] Junjun Jiang, Zengyuan Zuo, Gang Wu, Kui Jiang, and Xianming Liu. A survey on all-in-one image restoration: Taxonomy, evaluation and future trends. *arXiv preprint arXiv:2410.15067*, 2024. 1

- [32] M.I. Jordan and R.A. Jacobs. Hierarchical mixtures of experts and the em algorithm. In *Proceedings of 1993 International Conference on Neural Networks (IJCNN-93-Nagoya, Japan)*, 1993. 3
- [33] Orest Kupyn, Tetiana Martyniuk, Junru Wu, and Zhangyang Wang. Deblurgan-v2: Deblurring (orders-of-magnitude) faster and better. In *ICCV*, 2019. 1, 3
- [34] FirstName LastName. The frobnicatable foo filter, 2014. Face and Gesture submission ID 324. Supplied as supplemental material fg324.pdf.
- [35] FirstName LastName. Frobnication tutorial, 2014. Supplied as supplemental material tr.pdf.
- [36] Dmitry Lepikhin, HyoukJoong Lee, Yuanzhong Xu, Dehao Chen, Orhan Firat, Yanping Huang, Maxim Krikun, Noam Shazeer, and Zhifeng Chen. {GS}hard: Scaling giant models with conditional computation and automatic sharding. In *ICLR*, 2021. 3
- [37] Mike Lewis, Shruti Bhosale, Tim Dettmers, Naman Goyal, and Luke Zettlemoyer. Base layers: Simplifying training of large, sparse models. In *NeurIPS*, 2021.
- [38] Boyi Li, Wenqi Ren, Dengpan Fu, Dacheng Tao, Dan Feng, Wenjun Zeng, and Zhangyang Wang. Benchmarking single-image dehazing and beyond. *IEEE TIP*, 28(1): 492–505, 2019. 5, 6, 7, 1
- [39] Boyun Li, Xiao Liu, Peng Hu, Zhongqin Wu, Jiancheng Lv, and Xi Peng. All-In-One Image Restoration for Unknown Corruption. In *CVPR*, 2022. 1, 3, 6, 7
- [40] Chongyi Li, Chunle Guo, Wenqi Ren, Runmin Cong, Junhui Hou, Sam Kwong, and Dacheng Tao. An underwater image enhancement benchmark dataset and beyond. *IEEE TIP*, 29:4376–4389, 2020.
- [41] Junnan Li, Dongxu Li, Caiming Xiong, and Steven C. H. Hoi. BLIP: bootstrapping language-image pre-training for unified vision-language understanding and generation. In *ICML*, 2022. 4
- [42] Junnan Li, Dongxu Li, Silvio Savarese, and Steven C. H. Hoi. BLIP-2: bootstrapping language-image pre-training with frozen image encoders and large language models. In *ICML*, 2023. 4
- [43] Junyi Li, Zhilu Zhang, Xiaoyu Liu, Chaoyu Feng, Xiaotao Wang, Lei Lei, and Wangmeng Zuo. Spatially adaptive self-supervised learning for real-world image denoising. In *CVPR*, 2023.
- [44] Junyi Li, Zhilu Zhang, and Wangmeng Zuo. Tbsn: Transformer-based blind-spot network for self-supervised image denoising. *arXiv preprint arXiv:2404.07846*, 2024.
- [45] Youwei Li, Haibin Huang, Lanpeng Jia, Haoqiang Fan, and Shuaicheng Liu. D2c-sr: A divergence to convergence approach for real-world image super-resolution. In *ECCV*, 2022. 1, 3
- [46] Jingyun Liang, Jie Zhang Cao, Guolei Sun, Kai Zhang, Luc Van Gool, and Radu Timofte. Swinir: Image restoration using swin transformer. In *ICCVW*, 2021. 1, 3, 6, 7, 8
- [47] Jie Liang, Hui Zeng, and Lei Zhang. Efficient and degradation-adaptive network for real-world image super-resolution. In *ECCV*, 2022. 1, 3
- [48] Bee Lim, Sanghyun Son, Heewon Kim, Seungjun Nah, and Kyoung Mu Lee. Enhanced deep residual networks for single image super-resolution. In *CVPRW*, 2017. 6
- [49] Jingbo Lin, Zhilu Zhang, Yuxiang Wei, Dongwei Ren, Dongsheng Jiang, Qi Tian, and Wangmeng Zuo. Improving image restoration through removing degradations in textual representations. In *CVPR*, 2024. 1
- [50] Lin Liu, Lingxi Xie, Xiaopeng Zhang, Shanxin Yuan, Xiangyu Chen, Wengang Zhou, Houqiang Li, and Qi Tian. Tape: Task-agnostic prior embedding for image restoration. In *ECCV*, 2022. 6, 7
- [51] Xiaohui Liu, Zhilu Zhang, Xiaohe Wu, Chaoyu Feng, Xiaotao Wang, Lei Lei, and Wangmeng Zuo. Learning real-world image de-weathering with imperfect supervision. In *AAAI*, 2024. 1
- [52] Yihao Liu, Anran Liu, Jinjin Gu, Zhipeng Zhang, Wenhao Wu, Yu Qiao, and Chao Dong. Discovering distinctive "semantics" in super-resolution networks. *arXiv preprint arXiv:2108.00406*, 2022. 8
- [53] Yihao Liu, Jingwen He, Jinjin Gu, Xiangtao Kong, Yu Qiao, and Chao Dong. Degae: A new pretraining paradigm for low-level vision. In *CVPR*, 2023.
- [54] Yun-Fu Liu, Da-Wei Jaw, Shih-Chia Huang, and Jenq-Neng Hwang. Desnownet: Context-aware deep network for snow removal. *IEEE TIP*, 27(6):3064–3073, 2018. 1
- [55] Yun-Fu Liu, Da-Wei Jaw, Shih-Chia Huang, and Jenq-Neng Hwang. Desnownet: Context-aware deep network for snow removal. *IEEE TIP*, 27(6):3064–3073, 2018. 1, 5, 6, 7
- [56] Ze Liu, Yutong Lin, Yue Cao, Han Hu, Yixuan Wei, Zheng Zhang, Stephen Lin, and Baining Guo. Swin transformer: Hierarchical vision transformer using shifted windows. In *ICCV*, 2021. 1
- [57] Ziwei Luo, Fredrik K Gustafsson, Zheng Zhao, Jens Sjölund, and Thomas B Schön. Controlling vision-language models for universal image restoration. In *ICLR*, 2024. 4, 8
- [58] David R. Martin, Charless C. Fowlkes, Doron Tal, and Jitendra Malik. A database of human segmented natural images and its application to evaluating segmentation algorithms and measuring ecological statistics. In *ICCV*, 2001. 5, 6
- [59] Tom M Mitchell. *Machine learning*. 1997. 4
- [60] Basil Mustafa, Carlos Riquelme Ruiz, Joan Puigcerver, Rodolphe Jenatton, and Neil Houlsby. Multimodal contrastive learning with LIMoe: the language-image mixture of experts. In *NeurIPS*, 2022. 3
- [61] Seungjun Nah, Tae Hyun Kim, and Kyoung Mu Lee. Deep multi-scale convolutional neural network for dynamic scene deblurring. In *CVPR*, 2017. 1, 5, 6, 7
- [62] Seungjun Nah, Tae Hyun Kim, and Kyoung Mu Lee. Deep multi-scale convolutional neural network for dynamic scene deblurring. In *CVPR*, 2017. 7
- [63] Dongwon Park, Byung Hyun Lee, and Se Young Chun. All-in-one image restoration for unknown degradations using adaptive discriminative filters for specific degradations. In *CVPR*, 2023. 1, 3

- [64] Vaishnav Potlapalli, Syed Waqas Zamir, Salman Khan, and Fahad Khan. Promptir: Prompting for all-in-one image restoration. In *NeurIPS*, 2023. 1, 3, 5, 6, 7, 8, 2
- [65] Joan Puigcerver, Carlos Riquelme Ruiz, Basil Mustafa, and Neil Houlsby. From sparse to soft mixtures of experts. In *ICLR*, 2024. 3
- [66] Rui Qian, Robby T. Tan, Wenhan Yang, Jiajun Su, and Jiaying Liu. Attentive generative adversarial network for rain-drop removal from a single image. In *CVPR*, 2018.
- [67] Alec Radford, Jong Wook Kim, Chris Hallacy, Aditya Ramesh, Gabriel Goh, Sandhini Agarwal, Girish Sastry, Amanda Askell, Pamela Mishkin, Jack Clark, Gretchen Krueger, and Ilya Sutskever. Learning transferable visual models from natural language supervision. In *ICML*, 2021. 1
- [68] Samyam Rajbhandari, Conglong Li, Zhewei Yao, Minjia Zhang, Reza Yazdani Aminabadi, Ammar Ahmad Awan, Jeff Rasley, and Yuxiong He. Deepspeed-moe: Advancing mixture-of-experts inference and training to power next-generation ai scale. In *ICML*, 2022. 3
- [69] Dongwei Ren, Wangmeng Zuo, Qinghua Hu, Pengfei Zhu, and Deyu Meng. Progressive image deraining networks: A better and simpler baseline. In *CVPR*, 2019. 1, 3
- [70] Jaesung Rim, Haeyun Lee, Jucheol Won, and Sunghyun Cho. Real-world blur dataset for learning and benchmarking deblurring algorithms. In *ECCV*, 2020. 1
- [71] Carlos Riquelme Ruiz, Joan Puigcerver, Basil Mustafa, Maxim Neumann, Rodolphe Jenatton, André Susano Pinto, Daniel Keysers, and Neil Houlsby. Scaling vision with sparse mixture of experts. In *Advances in Neural Information Processing Systems*, 2021. 3
- [72] Noam Shazeer, \*Azalia Mirhoseini, \*Krzysztof Maziarz, Andy Davis, Quoc Le, Geoffrey Hinton, and Jeff Dean. Outrageously large neural networks: The sparsely-gated mixture-of-experts layer. In *ICLR*, 2017. 3, 5
- [73] H.R. Sheikh, Z.Wang, L. Cormack, and A.C. Bovik. Live image quality assessment database release 2. <http://live.ece.utexas.edu/research/quality>. 5, 6, 7
- [74] Sheng Shen, Zhewei Yao, Chunyuan Li, Trevor Darrell, Kurt Keutzer, and Yuxiong He. Scaling vision-language models with sparse mixture of experts. In *EMNLP*, 2023. 3
- [75] Karen Simonyan and Andrew Zisserman. Very deep convolutional networks for large-scale image recognition. In *ICLR*, 2015. 8
- [76] Yuda Song, Zhuqing He, Hui Qian, and Xin Du. Vision transformers for single image dehazing. *IEEE TIP*, 32:1927–1941, 2023. 1, 3
- [77] Yujing Sun, Yizhou Yu, and Wenping Wang. Moiré photo restoration using multiresolution convolutional neural networks. *IEEE TIP*, 27(8):4160–4172, 2018.
- [78] Yuchuan Tian, Jianhong Han, Hanting Chen, Yuanyuan Xi, Guoyang Zhang, Jie Hu, Chao Xu, and Yunhe Wang. Instruct-ipt: All-in-one image processing transformer via weight modulation. *arXiv preprint arXiv:2407.00676*, 2024. 2, 3
- [79] Jeya Maria Jose Valanarasu, Rajeev Yasarla, and Vishal M. Patel. Transweather: Transformer-based restoration of images degraded by adverse weather conditions. In *CVPR*, 2022. 1, 3, 6, 7
- [80] Ashish Vaswani, Noam Shazeer, Niki Parmar, Jakob Uszkoreit, Llion Jones, Aidan N Gomez, Łukasz Kaiser, and Illia Polosukhin. Attention is all you need. In *NeurIPS*, 2017. 1
- [81] Feng Wang, Jian Cheng, Weiyang Liu, and Haijun Liu. Additive margin softmax for face verification. *IEEE Signal Processing Letters*, 2018.
- [82] Xintao Wang, Liangbin Xie, Chao Dong, and Ying Shan. Real-esrgan: Training real-world blind super-resolution with pure synthetic data. In *ICCVW*, 2021. 1
- [83] Chen Wei, Wenjing Wang, Wenhan Yang, and Jiaying Liu. Deep retinex decomposition for low-light enhancement. In *BMVC*, 2018. 1, 5, 6, 7
- [84] Zhang Wenlong, Li Xiaohui, Guangyuan SHI, Chen Xiangyu, Qiao Yu, Zhang Xiaoyun, Wu Xiao-Ming, and Dong Chao. Real-world image super-resolution as multi-task learning. In *NeurIPS*, 2023. 1, 3
- [85] Lemeng Wu, Mengchen Liu, Yinpeng Chen, Dongdong Chen, Xiyang Dai, and Lu Yuan. Residual mixture of experts. *arXiv preprint arXiv:2204.09636*, 2022.
- [86] Xun Wu, Shaohan Huang, and Furu Wei. Mixture of LoRA experts. In *ICLR*, 2024.
- [87] Kong Xiangtao, Dong Chao, and Zhang Lei. Towards effective multiple-in-one image restoration: A sequential and prompt learning strategy. *arXiv preprint arXiv:2401.03379*, 2024. 1, 3, 6, 8
- [88] Liangbin Xie, Xintao Wang, Chao Dong, Zhongang Qi, and Ying Shan. Finding discriminative filters for specific degradations in blind super-resolution. In *NeurIPS*, 2021.
- [89] Xiaogang Xu, Ruixing Wang, Chi-Wing Fu, , and Jiaya Jia. Snr-aware low-light image enhancement. In *CVPR*, 2022. 1, 6, 8
- [90] Yimin Xu, Nanxi Gao, Yunshan Zhong, Fei Chao, and Rongrong Ji. Unified-width adaptive dynamic network for all-in-one image restoration. *arXiv preprint arXiv:2405.15475*, 2024. 1, 3
- [91] Qinhong Yang, Dongdong Chen, Zhentao Tan, Qiankun Liu, Qi Chu, Jianmin Bao, Lu Yuan, Gang Hua, and Nenghai Yu. Hq-50k: A large-scale, high-quality dataset for image restoration. *arXiv preprint arXiv:2306.05390*, 2023. 1, 3
- [92] Wenhan Yang, Robby T. Tan, Jiashi Feng, Jiaying Liu, Zongming Guo, and Shuicheng Yan. Deep joint rain detection and removal from a single image. In *CVPR*, 2017. 5, 6, 7
- [93] Eduard Zamfir, Zongwei Wu, Nancy Mehta, Danda Dani Paudel, Yulun Zhang, and Radu Timofte. Efficient degradation-aware any image restoration. *arXiv preprint arXiv:2405.15475*, 2024. 3
- [94] Syed Waqas Zamir, Aditya Arora, Salman Khan, Munawar Hayat, Fahad Shahbaz Khan, Ming-Hsuan Yang, and Ling Shao. Multi-stage progressive image restoration. In *CVPR*, 2021. 1, 3, 6, 7, 8

- [95] Syed Waqas Zamir, Aditya Arora, Salman Khan, Munawar Hayat, Fahad Shahbaz Khan, and Ming-Hsuan Yang. Restormer: Efficient transformer for high-resolution image restoration. In *CVPR*, 2022. 1, 3, 6, 7, 8, 2
- [96] He Zhang and Vishal M. Patel. Density-aware single image de-raining using a multi-stream dense network. In *CVPR*, 2018. 1, 7
- [97] Jinghao Zhang, Jie Huang, Mingde Yao, Zizheng Yang, Hu Yu, Man Zhou, and Feng Zhao. Ingredient-oriented multi-degradation learning for image restoration. In *CVPR*, 2023. 1, 3, 5, 6, 7
- [98] Kai Zhang, Wangmeng Zuo, Yunjin Chen, Deyu Meng, and Lei Zhang. Beyond a gaussian denoiser: Residual learning of deep CNN for image denoising. *IEEE TIP*, 26(7):3142–3155, 2017. 1, 3
- [99] Kai Zhang, Wangmeng Zuo, and Lei Zhang. Learning a single convolutional super-resolution network for multiple degradations. In *CVPR*, 2018. 1
- [100] Kai Zhang, Jingyun Liang, Luc Van Gool, and Radu Timofte. Designing a practical degradation model for deep blind image super-resolution. In *ICCV*, 2021. 1
- [101] Lei Zhang, Xiaolin Wu, Antoni Buades, and Xin Li. Color demosaicking by local directional interpolation and non-local adaptive thresholding. *J. Electronic Imaging*, 20(2):023016, 2011.
- [102] Ruofan Zhang, Jinjin Gu, Haoyu Chen, Chao Dong, Yulun Zhang, and Wenming Yang. Crafting training degradation distribution for the accuracy-generalization trade-off in real-world super-resolution. In *ICML*, 2023.
- [103] Wenlong Zhang, Guangyuan Shi, Yihao Liu, Chao Dong, and Xiao-Ming Wu. A closer look at blind super-resolution: Degradation models, baselines, and performance upper bounds. In *CVPRW*, 2022. 1
- [104] Xinyi Zhang, Hang Dong, Jinshan Pan, Chao Zhu, Ying Tai, Chengjie Wang, Jilin Li, Feiyue Huang, and Fei Wang. Learning to restore hazy video: A new real-world dataset and a new method. In *CVPR*, pages 9239–9248, 2021.
- [105] Yabo Zhang, Yuxiang Wei, Dongsheng Jiang, Xiaopeng Zhang, Wangmeng Zuo, and Qi Tian. Controlvideo: Training-free controllable text-to-video generation. *arXiv preprint arXiv:2305.13077*, 2023. 1
- [106] Zhilu Zhang, Haolin Wang, Ming Liu, Ruohao Wang, Jiawei Zhang, and Wangmeng Zuo. Learning raw-to-srgb mappings with inaccurately aligned supervision. In *ICCV*, 2021. 1
- [107] Zhilu Zhang, Rongjian Xu, Ming Liu, Zifei Yan, and Wangmeng Zuo. Self-supervised image restoration with blurry and noisy pairs. In *NeurIPS*, 2022. 1
- [108] Zhilu Zhang, Shuhao Zhang, Renlong Wu, Zifei Yan, and Wangmeng Zuo. Bracketing is all you need: Unifying image restoration and enhancement tasks with multi-exposure images. *arXiv preprint arXiv:2401.00766*, 2024. 1
- [109] Zihan Zhong, Zhiqiang Tang, Tong He, Haoyang Fang, and Chun Yuan. Convolution meets loRA: Parameter efficient finetuning for segment anything model. In *ICLR*, 2024.
- [110] Yuqian Zhou, David Ren, Neil Emerton, Sehoon Lim, and Timothy Large. Image restoration for under-display camera. In *CVPR*, 2021.
- [111] Jinguo Zhu, Xizhou Zhu, Wenhai Wang, Xiaohua Wang, Hongsheng Li, Xiaogang Wang, and Jifeng Dai. Uni-perceiver-moe: Learning sparse generalist models with conditional moes. In *NeurIPS*, 2022. 3
- [112] Yurui Zhu, Tianyu Wang, Xueyang Fu, Xuanyu Yang, Xin Guo, Jifeng Dai, Yu Qiao, and Xiaowei Hu. Learning weather-general and weather-specific features for image restoration under multiple adverse weather conditions. In *CVPR*, 2023. 1, 3, 8
- [113] Barret Zoph, Irwan Bello, Sameer Kumar, Nan Du, Yanping Huang, Jeff Dean, Noam Shazeer, and William Fedus. St-moe: Design stable and transferable sparse expert models. *arXiv preprint arXiv:2202.08906*, 2022. 3